MOLECULAR PHYSICS, 1979, VOL. 38, NO. 2, 625–655

Effects of laser linewidth on coherent antiStokes Raman spectroscopy

by M. A. YURATICH
Department of Electronics, The University, Southampton, SO9 5NH, U.K.

(*Received* 22 *December* 1978)

Expressions for the generated antiStokes spectral density in coherent antiStokes Raman spectroscopy (CARS) are obtained, which take into account the finite linewidths of laser sources and which may be used to analyse observed spectra. Lorentzian and gaussian laser lineshapes are taken as special cases, which enable further analytic results for single and multiline CARS spectra to be derived. Emphasis is placed on scanning and broadband (multiplex) CARS techniques, and the choice of laser sources discussed from the spectral point of view. As examples of multiline spectra an analytical account of a periodic spectrum is presented and temperature measurement from Q-branch spectra is treated.

1. INTRODUCTION

Coherent antiStokes Raman Spectroscopy (CARS) is now well-established as a technique complementary to spontaneous Raman spectroscopy (see for example the reviews [1–4]). Among its advantages are the easy detectability of the strong collimated antiStokes signals, which are free of background fluorescence, and the ability to monitor given spatial portions of the medium. The broadband (or multiplex) technique, in which a broadband Stokes signal is injected into the medium [1–6], makes it possible to obtain a spectrum of several Raman lines in a single pulse. Thus by analysing the spectrum one can make temporally and spatially resolved measurements of density and temperature. This has obvious applications in investigations of turbulent media, such as flames, and fast reactions [2, 6, 7]. By suitable choice of narrow linewidth laser sources, both the broadband and conventional scanning CARS techniques allow high-resolution (compared to spontaneous Raman spectroscopy) spectra to be obtained, assisted by the partial Doppler-cancellation that occurs with forward scattering.

As in any spectroscopic technique, one ultimately relies on the ability to analyse the recorded spectra and, particularly in CARS, this implies that proper account be taken of the laser linewidths. Surprisingly, however, little work has been done in this area, the CARS theory usually idealizing the lasers as being monochromatic or infinitely broad, as appropriate, and thus scarcely taking account of the far from transform-limited nature of most laser sources. It is intuitively obvious that, for high resolution, at least some of the lasers should have linewidths much less than the Raman lines of interest. If investigations are limited to a few species, then this can usually be arranged by careful design, though it is desirable even then to quantify ' much less than ' for a single Raman

0026–8976/79/3802 0625 $02.00

line. In the case of a set of lines, however, the effect of laser linewidth is not immediately apparent when the line spacing is comparable to or smaller than the Raman linewidth. Moreover, if CARS is to become a routine spectroscopic method, then there will always be species for which the Raman linewidths and/or line spacings will be comparable to the laser linewidths. This is further complicated when for example a temperature measurement is taken. The temperature is a fitting parameter in the analysis of the spectrum. Over the entire spectrum some lines may be more heavily weighted than others, and it may be these alone for which the laser linewidth must be narrow. There are indeed some cases in temperature and density measurements where it will be seen that the result is independent of laser linewidth, rendering the use of narrow linewidth sources unnecessary.

In this paper a theoretical discussion of the effects of laser linewidth on CARS spectra is presented and is intended to apply to the most common experimental arrangements, in which cw or conventional pulsed laser sources (several ns duration) are employed; thus transform-limited picosecond-pulse CARS techniques are excluded. The principal simplifying assumption which may then be made is that the laser linewidths arise from stationary, normal (gaussian), stochastic amplitude and phase fluctuations. As will be seen, this incoherence in the sources results in the expression for the antiStokes spectral intensity reducing essentially to that of a convolution over laser lineshapes of the usual monochromatic wave formulae.

The body of the paper commences (§ 2) with a review of the formal theory of CARS, and the usual solutions in the idealized laser source approximation. Both the susceptibility and material excitation viewpoints are considered and shown to be equivalent even for arbitrary time variations of the sources; the former method is however used as the basis of the later analysis. In § 3 the antiStokes spectrum is derived as an explicit function of stochastic laser linewidth spectra, as mentioned above. The derivation of this result is made possible mainly because of the parametric nature of CARS, that is the antiStokes signal depends on the prescribed injected waves and not itself. (The corresponding theory for the, at first sight, more simple non-parametric process of stimulated Raman scattering, with its single injected pump wave, is made much more difficult to analyse because of the dependence of the Stokes signal growth rate on itself, [8, 9].) The result is discussed in general terms for the scanning and broadband methods, and a new CARS arrangement for the latter technique is pointed out. Then in § 4 two specific laser spectra are introduced, lorentzian and gaussian. These are used to investigate a single Raman line, for which simple results are deduced. In § 5 these laser lineshapes are applied to multiline spectra, including the non-resonant background. The resulting expressions form a useful starting point for the analysis of real CARS spectra, since the lasers are each characterized analytically by one parameter, their linewidth, as opposed to the more general expressions in § 3. Two multiline spectra are then discussed, in § 6, a periodic Raman spectrum (that is equally spaced lines of equal amplitude and linewidth), for which a particularly simple result is found after analytic summation over all the lines, and in § 7 the Q-branch of a diatomic molecule. These spectra were chosen in order to show as simply as possible the effect of laser linewidth on multiline spectra for varying line spacings and, in the example of § 7, on temperature measurements. The paper is concluded

in § 8 with a discussion of the relative merits of the various CARS techniques from the point of view of constraints on the laser sources.

2. Summary of CARS theory

Figure 1 depicts the arrangement for the most general CARS process, in which three signals are injected, at frequencies centred around ω_1^0, ω_s^0 and ω_2^0. The Stokes ω_s^0 and pump ω_1^0 frequencies are tuned into Raman resonance with a Raman transition $g \rightarrow f$, of frequency Ω_{fg}, that is the detuning Δ is small, where $\Delta = \Omega_{fg} + \omega_s^0 - \omega_1^0$. These waves set up a strong excitation in the medium which thus results in a strongly oscillating polarizability at the driving-force frequency $\omega_d^0 \equiv \omega_1^0 - \omega_s^0 = \Omega_{fg} - \Delta \simeq \Omega_{fg}$. Consequently the polarization induced in the medium by the probe (or second pump) wave, frequency ω_2^0, has a sideband at the antiStokes frequency $\omega_{as}^0 = \omega_2^0 + (\omega_1^0 - \omega_s^0) \simeq \Omega_{fg} + \omega_2^0$. The experimental conditions are usually such that other sidebands may be ignored and that stimulated Raman processes remain well below threshold.

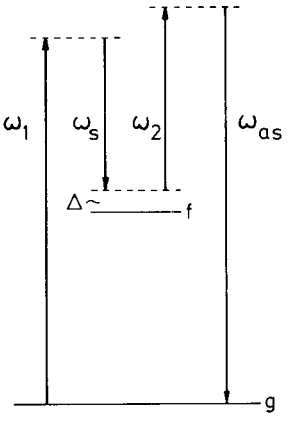

Figure 1. Notations used to describe CARS. The frequencies ω_1, ω_s, ω_2 and ω_{as} contained within the spread of the laser linewidths are centred around ω_1^0, ω_s^0, ω_2^0 and $\omega_{as}^0 \equiv \omega_d^0 + \omega_2^0$, respectively. The driving-force frequency is $\omega_d^0 = \omega_1^0 - \omega_s^0$ and the detuning from Raman resonance is $\Delta = \Omega_{fg} + \omega_s^0 - \omega_1^0 = \Omega_{fg} - \omega_d^0$, depicted here as negative, where Ω_{fg} is the Raman shift.

The total electric field $E(t)$ in the medium is a superposition of the input and generated waves $E_{1,s,2,as}(t)$, where for the present any spatial dependence is suppressed. The Fourier transform $E(\omega)$ of $E(t)$ is given by

$$E(t) = \int E(\omega) \exp(-i\omega t)\, d\omega\,; \quad E(\omega) = E(-\omega)^*, \tag{1 a}$$

(unless explicitly indicated otherwise, all integrations range from $-\infty$ to ∞ throughout the paper). This transform may be written as the superposition

$$E(\omega) = \tfrac{1}{2}\{E_1(\omega) + E_s(\omega) + E_2(\omega) + E_{as}(\omega)\}, \tag{1 b}$$

where

$$E_1(t) = \tfrac{1}{2} \int E_1(\omega_1) \exp(-i\omega_1 t)\, d\omega_1, \tag{1 c}$$

etc. The quantity $E_1(\omega_1)$ is sharply peaked around the frequencies $\pm\omega_1^0$, since it is the transform of an optical carrier wave of frequency ω_1^0, modulated

by a slowly-time-varying (complex) envelope $A_1(t)$

$$E_1(t) = \tfrac{1}{2}A_1(t)\exp(-i\omega_1{}^0 t) + \text{cc.} \tag{2a}$$

Thus

$$E_1(\omega_1) = A_1(\omega_1 - \omega_1{}^0) + A_1(-\omega_1 - \omega_1{}^0)^*. \tag{2b}$$

Notice that the transform $A_1(\omega)$ is sharply peaked around $\omega = 0$; and that except when $E_1(\omega_1)$ is real, $A_1(\omega) \neq A_1(-\omega)^*$. For all practical purposes

$$E_1(\omega_1) = A_1(\omega_1 - \omega_1{}^0) \qquad \omega_1 > 0, \tag{2c}$$

$$= A_1(-\omega_1 - \omega_1{}^0)^* \quad \omega_1 < 0. \tag{2d}$$

The spectral density of E_1 is given by

$$S_1(\omega_1) = \tfrac{1}{2}\epsilon_0 c\eta_1{}^0 \int \langle E_1(\omega_1)^* E_1(\omega_1 + \omega)\rangle \, d\omega, \tag{3}$$

where $\eta_1{}^0$ is the refractive index at frequency $\omega_1{}^0$ and the brackets $\langle\ \rangle$ denote an ensemble average. In later sections all of the fields will be stationary and so the correlation function in (3) will then be proportional to $\delta(\omega)$. Hence $S_1(\omega_1) \sim \langle |E_1(\omega_1)|^2 \rangle$ and is the intensity per unit bandwidth of the wave. A trivial example of this is afforded when $E_1(t)$ is a monochromatic wave. Then $E_1(\omega_1) = E_1\delta(\omega_1 - \omega_1{}^0) + E_1{}^* \, \delta(\omega_1 + \omega_1{}^0)$ and $S_1(\omega_1) = I_1{}^0 \, \delta(\omega_1 - \omega_1{}^0)$, $\omega_1 > 0$, where $I_1{}^0 = \tfrac{1}{2}\epsilon_0 c\eta_1{}^0 |E_1|^2$ is the intensity of the wave. Since $S_1(\omega_1) = S_1(-\omega_1)$, when giving expressions for spectral densities we will only consider positive frequencies.

The third order non-linear antiStokes polarization $P_{as}(t)$, oscillating around $\omega_{as}{}^0 = \omega_1{}^0 + \omega_2{}^0 - \omega_s{}^0$, can be written in terms of $P_{as}(\omega_{as})$ analogously to (1 c)–(2) and one finds, in terms of the non-linear susceptibility $\chi^{(3)}$ (units $\text{m}^2\ \text{V}^{-2}$),

$$P_{as}(\omega_{as}) = \tfrac{3}{2}\epsilon_0 \int \chi^{(3)}(-\omega_{as}\,;\ \omega_2, \omega_1, -\omega_s) E_2(\omega_2) E_1(\omega_1) E_s(\omega_s)^* \times \delta(\omega_{as} - \omega_2 - \omega_1 + \omega_s)\, d\omega_2\, d\omega_1\, d\omega_s. \tag{4}$$

(The numerical factor has been discussed at length in, for example, [10].) For monochromatic waves (4) reduces to

$$P_{as}(\omega_{as}) = \tfrac{3}{2}\epsilon_0 \chi^{(3)}(-\omega_{as}{}^0\,;\ \omega_2{}^0, \omega_1{}^0, -\omega_s{}^0) E_2 E_1 E_s{}^* \, \delta(\omega_{as} - \omega_{as}{}^0), \quad \omega_{as} > 0 \tag{5}$$

where E_1, E_2, $E_s{}^*$ are the field amplitudes.

The CARS susceptibility is given by

$$\chi^{(3)}(-\omega_{as}\,;\ \omega_2, \omega_1, -\omega_s) = \chi_{\text{NR}} + \sum \frac{N/6\hbar\epsilon_0}{\Omega_{fg} + \omega_s - \omega_1 - i\Gamma_{fg}} \times [\overline{\rho(g)} - \overline{\rho(f)}]\overline{\alpha_{\text{CARS}}{}^* \, \alpha_{\text{R}}}, \tag{6}$$

where N is the number density of molecules, $\overline{\rho(g)}$ is the fraction of molecules in the states g of energy $\hbar\Omega_g$, Γ_{fg} is the HWHM spontaneous Raman linewidth of the Raman transition $g \to f$, $\overline{\alpha_{\text{CARS}}{}^* \, \alpha_{\text{R}}}$ is the orientation averaged product of two two-photon matrix elements, χ_{NR} is a background contribution from non-resonant transitions and $\sum$ denotes a sum over resonant Raman lines. The susceptibility depends, through α_{R} and α_{CARS}, on the polarization vectors of the waves and on the selection rules for the transitions $g \to f$, and has been fully discussed in this respect in [11]. In addition, α_{R} and α_{CARS} are respectively

dependent on the frequency pairs $-\omega_s$; ω_1 and $-\omega_2$; ω_{as}. This dependence will be neglected here, since except in extreme examples of resonance CARS, α_R and α_{CARS} are essentially constant for frequencies within the spread of the laser linewidths. The frequency dependence of the susceptibility is thus given by the resonant denominators in (6). For simplicity, but with no great restriction, we will assume that there is only one isolated line of interest and no background contribution ($\chi_{NR}=0$) until § 5. Thus (6) may be replaced by

$$\chi^{(3)}(-\omega_{as};\ \omega_2, \omega_1,\ -\omega_s) \simeq \hat{\chi}_{CARS} L_\Gamma(\Omega+\omega_s-\omega_1), \tag{7 a}$$

where Ω is the transition frequency, Γ its linewidth,

$$\hat{\chi}_{CARS} = N[\overline{\rho(g)} - \overline{\rho(f)}]\overline{\alpha_{CARS}^*\, \alpha_R}/6\hbar\epsilon_0\Gamma. \tag{7 b}$$

and

$$L_\Gamma(x) = \Gamma/(x-i\Gamma). \tag{7 c}$$

Equations (4) and (6) represent the formal susceptibility theory of the CARS polarization. A more direct physical approach is afforded by pursuing the notion of material excitation [1–3, 10, 12–13] used in the qualitative introduction to this section. An example of this excitation is a vibrational coordinate displacement $Q_\Omega(t)$ (dimensionless) of natural frequency Ω, though more generally it is the off-diagonal density matrix element for the Raman transition. Similarly to (2 *a*), $Q_\Omega(t)$ may be written

$$Q_\Omega(t) = Q(t)\exp(-i\omega_d{}^0 t) + \text{cc};\quad \omega_d{}^0 = \omega_1{}^0 - \omega_s{}^0, \tag{8}$$

where $Q(t)$ is slowly-time-varying. Then the forced harmonic oscillator equation for $Q_\Omega(t)$ reduces to

$$\frac{\partial Q_\Omega(t)}{\partial t} + i(\Delta - i\Gamma)Q(t) = \frac{i\alpha_R}{4\hbar} A_1(t)A_s(t)^*, \tag{9}$$

where $\alpha_R = (\partial\alpha/\partial Q_\Omega)_0$, the equilibrium polarizability derivative, and $\Delta = \Omega + \omega_s{}^0 - \omega_1{}^0 = \Omega - \omega_d{}^0$ as before. The polarization envelope is given by

$$P_{as}(t) = N\alpha_{CARS}^*\, Q(t)A_2(t), \tag{10}$$

where in this classical description α_{CARS} is real, and equal to α_R, assuming for example that the unit polarization vectors of the waves are the same [11]. For monochromatic waves the solution of (9)–(10) is trivial and leads to (5) and (6) [12]. We now demonstrate for arbitrary envelopes $A_1(t)$, $A_s(t)$, $A_2(t)$ that (9)–(10) are equivalent to the general expression (4). Taking Fourier transforms, where $Q(t) \to Q(\omega)$ defined as in (1 *a*), gives

$$Q(\omega) = (i\alpha_R/4\hbar)\int A_1(\omega_1)A_s(\omega_1-\omega)^*\, d\omega_1/(\Delta-\omega-i\Gamma) \tag{11}$$

and

$$\begin{aligned} P_{as}(\omega_{as}) &= N\alpha_{CARS}^* \int Q(\omega)A_2(\omega_{as}-\omega)\, d\omega \\ &= \frac{N\alpha_{CARS}^*\, \alpha_R}{4\hbar}\int \frac{A_1(\omega_1)A_2(\omega_{as}-\omega)A_s(\omega_1-\omega)}{\Delta-\omega-i\Gamma}\, d\omega_1\, d\omega. \end{aligned} \tag{12}$$

Use of the identity

$$A_2(\omega_{as}-\omega)A_s(\omega_1-\omega)^* = A_2(\omega_2)A_s(\omega_s)^*\ \delta(\omega_{as}-\omega_1-\omega_2+\omega_s)\delta(\omega+\omega_s-\omega_1)$$

in (12) then gives (4). Since we wish to find the antiStokes spectrum, it proves more convenient to work with (4) rather than (9)–(10); some corresponding equations based on the latter are however given in Appendix A for comparison, and (11) will later be used to derive the excitation spectrum.

For an isotropic medium with plane waves co-propagating in the z-direction, the growth of the antiStokes wave is given by (see for example [10, 13] or [1–3])

$$\frac{\partial}{\partial z} A_{as}(\omega_{as}-\omega_{as}{}^0, z)=\frac{i\omega_{as}{}^0}{2\epsilon_0 c} P_{as}(\omega_{as}-\omega_{as}{}^0, z) \exp(-ik(\omega_{as})z), \tag{13}$$

where for the propagation problem the definitions (1)–(2) are extended to include the z-coordinate. Thus

$$E_{as}(z, t)=\tfrac{1}{2}A_{as}(z, t) \exp[i(k_{as}{}^0 z-\omega_{as}{}^0 t)]+\text{cc}, \tag{14}$$

where $A_{as}(z, t)$ is a slowly-time-and-space-varying envelope function, the wavevector $k_{as}{}^0$ equals $k_{as}(\omega_{as}{}^0)$, and $k_{as}(\omega_{as})=\eta(\omega_{as})\omega_{as}/c$; $\eta(\omega_{as})$ is the refractive index at frequency ω_{as} (but note $\eta_{as}{}^0\equiv\eta_{as}(\omega_{as}{}^0)$, cf. (3)). As discussed earlier, stimulated Raman scattering may be ignored, and so the input waves may be taken to be prescribed. Thus $A_{1,2,s}(z, t)=A_{1,2,s}(0, t)=A_{1,2,s}(t)$ as before. Equation (13) with (4) is then immediately integrable and yields

$$E_{as}(\omega_{as}, z)=\frac{3\omega_{as}{}^0}{4c}\int\left(\frac{\exp(i\Delta kz)-1}{\Delta k}\right)\chi^{(3)}(-\omega_{as}; \omega_2, \omega_1, -\omega_s) \times E_2(\omega_2)E_1(\omega_1)E_s(\omega_s)^*\,\delta(\omega_{as}-\omega_2-\omega_1-\omega_s)\,d\omega_2\,d\omega_1\,d\omega_s. \tag{15}$$

The phase mismatch Δk is given by

$$\Delta k=k_1(\omega_1)+k_2(\omega_2)-k_s(\omega_s)-k_{as}(\omega_{as}). \tag{16}$$

We will assume now and subsequently that for the given interaction length z the product Δkz varies negligibly within each of the regions for which the integrand in (15) is significant. Then Δk may be replaced by $\Delta k^0=k_1{}^0+k_2{}^0-k_3{}^0-k_{as}{}^0$ and the factor $(\exp(i\Delta k^0 z/2)-1)/\Delta k^0$ brought outside the integral sign. Except for resonant CARS, where the linear dispersion may be significant when a broad line (or several close ones) is probed by a broad laser spectrum, the error is unlikely to be important, particularly in view of the related experimental uncertainties in focusing and spatial homogeneity of the waves. Note, however, that the broad dependence of Δk on frequency is retained through Δk^0, although this does not affect the local spectral properties of the antiStokes wave, only its overall magnitude. This is the case even for the broadband technique, since each Raman line is efficiently excited by only a limited portion of the laser spectrum, comparable to the Raman linewidth. If desired, a different Δk^0 may be associated with different portions of the Raman spectrum for the broadband method to simulate the global variation of Δk. Nevertheless for convenience the variation of Δk^0 over a wide spectral range will be ignored, since we are interested in finer details of the antiStokes spectrum; in any case this is usually a good approximation.

The solution of (15) when all the waves are monochromatic is

$$I_{as}{}^0(z)=\frac{\eta_{as}{}^0}{\eta_1{}^0\,\eta_s{}^0\,\eta_2{}^0}\left|\frac{3\omega_{as}{}^0}{2c^2\,\epsilon_0} \times\chi^{(3)}(-\omega_{as}{}^0;\ \omega_2{}^0, \omega_1{}^0, -\omega_s{}^0)\,\frac{\sin(\Delta k^0 z/2)}{\Delta k^0/2}\right|^2 I_1{}^0\,I_s{}^0\,I_2{}^0. \tag{17a}$$

Equation (17 *a*) forms the basis of most discussions of CARS presented in the literature for the scanning method. In practice, as $\omega_1{}^0-\omega_s{}^0$ is scanned (tuned through the Raman lines) the integrated antiStokes spectrum is monitored, $I_{as}{}^0(z)=\int S_{as}(\omega_{as}, z)\, d\omega_{as}$, which is approximated by (17 *a*), and the Raman spectrum formed by the variation in $I_{as}{}^0(z)$ as the scanning proceeds. The notation in (17 *a*) may be simplified by writing

$$\hat{I}_{as}=\frac{\eta_{as}{}^0}{\eta_1{}^0\,\eta_s{}^0\,\eta_2{}^0}\left|\frac{3\omega_{as}{}^0}{2c^2\,\epsilon_0}\,\hat{\chi}_{\mathrm{CARS}}\,\frac{\sin(\Delta k^0\, z/2)}{\Delta k^0/2}\right|^2 \bar{I}_1\bar{I}_s\bar{I}_2, \tag{18}$$

where the $\bar{I}_{1,2,s}$ are mean intensities and $\hat{\chi}_{\mathrm{CARS}}$ has been defined in (7). Thus for monochromatic waves $\bar{I}_1=I_1{}^0$ etc. and (17 *a*) becomes

$$I_{as}{}^0(z)=\hat{I}_{as}|\mathrm{L}_\Gamma(\Delta)|^2\,;\quad \Delta=\Omega+\omega_s{}^0-\omega_1{}^0. \tag{17 b}$$

The second important limit of (15) that is found in the literature is an idealized broadband technique ([1, 5] and references in § 1). Suppose waves ω_1 and ω_2 to be monochromatic. Then (15) becomes

$$S_{as}(\omega_{as})=\hat{I}_{as}|\mathrm{L}_\Gamma(\Omega+\omega_2{}^0-\omega_{as})|^2\, S_s(\omega_1{}^0+\omega_2{}^0-\omega_{as})/\bar{I}_s \tag{19}$$

for the antiStokes spectral density. Hence if the Stokes spectrum is broad, that is $S_s=$ constant, then the antiStokes spectrum is just that of the Raman line, through the factor $|\mathrm{L}_\Gamma|^2$. The physical interpretation of this result has in the past rested on the fact that the relation $\omega_{as}=\omega_1{}^0+\omega_2{}^0-\omega_s$ for the broadband method (see delta function in (15)) ensures that to each antiStokes frequency there corresponds a unique Stokes frequency and hence a unique frequency of excitation of the Raman transition, $\omega_1{}^0-\omega_s$.

However, the broadband method has a deeper explanation, which makes possible a wider range of application. The formalism (9)–(10) shows quite clearly how first the waves ω_1 and ω_s set up the material excitation and then that the excitation beats with the wave ω_2 to produce the antiStokes polarization. Hence the generation of the antiStokes signal depends on the excitation itself and not the details of the means by which the excitation was established. In particular, for CARS (9) shows that $Q(t)$ depends equally on $A_1(t)$ and $A_s(t)$, and therefore it is unnecessary to give either of these fields prominence relative to the other. Going to (11), a given component $Q(\omega)$ is made up of a convolution of the two waves ω_1 and ω_s: all frequencies ω_1 and ω_s such that their difference satisfies $\omega_1-\omega_s=\omega$ contribute to $Q(\omega)$ and neither wave need be monochromatic. Then the component $Q(\omega)$ is convoluted with the wave ω_2 to produce the antiStokes polarization (12). If ω_2 is monochromatic, then $P_{as}(\omega_{as})$ is proportional to $Q(\omega_{as}-\omega_2{}^0)$ and the antiStokes spectrum is again that of the Raman line, provided only that the convoluted spectrum of ω_1 and ω_s is broad. In other words it is sufficient for ω_2 to be monochromatic in order to select a Fourier component of the excitation and for ω_1 and ω_s together to be broad in order to ensure uniform excitation of the medium across its Raman line. The consequences of this will be discussed in the next section.

When one source acts for ω_1 and ω_2, then the subscripts 2 can be changed to 1 and the right-hand side of (17)–(19) multiplied by a factor $\frac{1}{4}$. (The use of a single source of a given intensity differs from that of two sources of the same frequency and intensity, and this is the origin of the numerical factor.)

3. AntiStokes spectrum

A typical dye laser pulse may be $\tau_p \sim 5$ ns in duration, with a linewidth of $\sim 0{\cdot}1\ \mathrm{cm}^{-1}$. This corresponds to fluctuations on a time scale of ~ 50 ps, that is ~ 100 fluctuations in one pulse. Thus, within broad limits, in a single pulse the medium samples a large ensemble of such fluctuations over a period long compared to typical Raman relaxation times $T_2 = 1/\Gamma$. There are of course possible exceptions, such as for extremely well stabilized narrow bandwidth lasers, which are essentially transform-limited, or for very narrow Raman lines ($T_2 \gtrsim \tau_p$) or where the laser exhibits a large degree of random mode-locking. However, for the majority of cases it is reasonable to approximate the input waves as stationary stochastic processes, and this we do.

The correlation functions thus take the form [14, 15]

$$\langle E_1(t) E_1(t+\tau)\rangle = s_1(\tau), \tag{20}$$

where the non-dependence on t (stationarity condition) indicates that the beginning and end of the laser pulse plays no role, which is just the condition implied by $\tau_p > T_2$, as mentioned above.

The Fourier transform of (20) yields

$$\tfrac{1}{2}\epsilon_0 c \eta_1{}^0 \langle E_1(\omega_1)^*\, E_1(\omega_1+\omega)\rangle = \delta(\omega) S_1(\omega_1), \tag{21}$$

where the delta function is characteristic of a stationary process [14, 15]. Equation (21) is the defining equation for the spectral density $S_1(\omega_1)$ and by integrating both sides over ω one finds the alternative form (3). We shall write spectral densities as a product of their mean intensity and spectrum

$$S_1(\omega_1) = \bar{I}_1 \mathrm{L}_1(\omega_1)\ ; \quad \tfrac{1}{2}\int \mathrm{L}_1(\omega_1)\, d\omega_1 = 1. \tag{22}$$

Notice that a perfectly monochromatic wave is also stationary and has a spectral density $S(\omega) = \bar{I}\delta(\omega - \omega_0)$ when $\omega > 0$; this fact was used in deriving (17)–(19).

Consider first the case when ω_1, ω_2 and ω_s are provided by separate sources, so that the three waves are statistically independent. One can then write down from (15) and (18)

$$\begin{aligned}
&\tfrac{1}{2}\epsilon_0 c \eta_{as}{}^0 \langle E_{as}(\omega_{as})^*\, E_{as}(\omega_{as}+\omega)\rangle \\
&\quad = (\hat{I}_{as}/\bar{I}_1\bar{I}_s\bar{I}_2) \int \mathrm{L}_\Gamma(\Omega+\omega_s-\omega_1)^*\, \mathrm{L}_\Gamma(\Omega+\omega_s{}'-\omega_1{}') \\
&\qquad \times \langle E_1(\omega_1{}^*) E_1(\omega_1{}')\rangle \langle E_2(\omega_2)^*\, E_2(\omega_2{}')\rangle \langle E_s(\omega_s) E_s(\omega_s{}')^*\rangle \\
&\qquad \times \delta(\omega_{as}-\omega_1-\omega_2+\omega_s)\delta(\omega_{as}+\omega-\omega_1{}'-\omega_2{}'+\omega_s{}') \\
&\qquad\qquad \times d\omega_1\, d\omega_2\, d\omega_s\, d\omega_1{}'\, d\omega_2{}'\, d\omega_s{}'.
\end{aligned} \tag{23}$$

Use of (21) in (23) and a little manipulation with delta functions using $\delta(a)\delta(b) = \delta(a \pm b)\delta(a)$ shows that as expected the antiStokes spectrum is stationary (it is proportional to $\delta(\omega)$) and then, integrating over ω, that the spectral density is

$$S_{as}(\omega_{as}) = \hat{I}_{as} \int |\mathrm{L}_\Gamma(\Omega+\omega_s-\omega_1)|^2\, \mathrm{L}_1(\omega_1) L_s(\omega_s) \mathrm{L}_2(\omega_{as}+\omega_s-\omega_1)\, d\omega_1\, d\omega_s. \tag{24}$$

Making the substitution $\omega_d = \omega_1 - \omega_s$ in (24) gives

$$S_{as}(\omega_{as}) = \hat{I}_{as} \int |\mathrm{L}_\Gamma(\Omega-\omega_d)|^2\, \mathrm{L}_d(\omega_d) \mathrm{L}_2(\omega_{as}-\omega_d)\, d\omega_d, \tag{25}$$

where the normalized ' driving-force ' spectral density is

$$\mathrm{L}_d(\omega_d) = \int \mathrm{L}_1(\omega_s-\omega_d) L_s(\omega_s)\, d\omega_s. \tag{26}$$

Equations (24)–(26) are the basic results of this paper and may in principle be used to analyse a measured antiStokes spectrum, given the laser line shapes. In practice it is probable that special cases will be used as starting points. To this end, for the remainder of this section we consider the general features of (24)–(26), with particular reference to scanning and broadband CARS, and in later sections we specialize to given laser lineshapes.

Equation (24) shows that the effect of the random fluctuations on the CARS process is to wash out the coherence between individual Fourier components of the fields and to give a result equivalent to a superposition of antiStokes intensities over many monochromatic-wave CARS processes. Thus (24) is a convolution of the monochromatic-wave result (17)–(18) over all frequencies satisfying $\omega_{as} = \omega_1 + \omega_2 - \omega_{as}$.

The form (25)–(26) makes explicit the remarks at the end of the previous section, viz. that the antiStokes spectrum depends on ω_1 and ω_s equally, through the appearance of a compound spectrum $L_d(\omega_d)$.

In the scanning technique the total antiStokes intensity is measured as a function of the detuning $\Delta = \Omega + \omega_s^0 - \omega_1^0 = \Omega - \omega_d^0$. Thus, using (24)

$$I_{as}(\Delta) = \int S_{as}(\omega_{as})\, d\omega_{as} = \hat{I}_{as} \int |L_\Gamma(\Omega - \omega_d)|^2\, L_d(\omega_d)\, d\omega_d. \tag{27}$$

Provided both ω_1 and ω_s are narrow, that is $L_d(\omega_d)$ is narrow, $I_{as}(\Delta)$ traces out the Raman lineshape. Thus, setting $L_d(\omega_d) = \delta(\omega_d - \omega_1^0 + \omega_s^0) = \delta(\omega_d - \omega_d^0)$, for $\omega_d > 0$

$$I_{as}(\Delta) = \hat{I}_{as} |L_\Gamma(\Delta)|^2; \quad L_d \text{ sharp.} \tag{28}$$

(N.B. For $\omega_d < 0$ the integration of (27) to give (28) results in a term in $L_\Gamma(\Omega + |\omega_d|)$, which is very small and was therefore ignored in (28). Similar terms arise in most of the later calculations and again will be omitted.) Equation (27) shows that the resolution of the Raman spectrum is *independent* of the linewidth of ω_2. Hence it is only necessary for ω_1 and ω_s to be narrow in order that the resolution be equivalent to the purely monochromatic-wave case (17).

Equation (25) is strictly speaking the rigorous expression to be used when considering broadband CARS and similarly (27) is the rigorous expression for the scanning method. However, the formulae (25) and (27) are not fully analogous and so we take the limit of (25) where L_d is much broader than the Raman line. This gives

$$S_{as}(\omega_{as}) \simeq \hat{I}_{as} L_d(\omega_d^0) \int |L_\Gamma(\Omega + \omega_2 - \omega_{as})|^2\, L_2(\omega_2)\, d\omega_2 \tag{29}$$

($\omega_2 = \omega_{as} - \omega_d$). The similarity between (27) and (29) is evident. For high resolution ω_2 is sharp and thus

$$S_{as}(\omega_{as}) \simeq \hat{I}_{as} L_d(\omega_d^0) |L_\Gamma(\Delta + \omega_{as}^0 - \omega_{as})|^2; \quad L_2 \text{ sharp.} \tag{30}$$

Since $\Delta + \omega_{as}^0 = \Omega + \omega_2^0$, (30) is equivalent to the broadband limit of (19) with the exception that $L_d(\omega_d^0)$ rather than $L_s(\omega_s^0)$ appears, reflecting the generality of the present treatment. The appearance of Δ in (30) (and implicitly in (29) through $\Omega - \omega_d$) is unimportant since, in the idealized limit to which (29)–(30) apply, Δ represents only an overall shift of the spectrum and may therefore be set to zero with no loss of generality. This is true also of a multiline spectrum. The detuning Δ only plays a role in the broadband case (or indeed in any experiment in which $S_{as}(\omega_{as})$ is measured) if L_d is not constant across the entire spectral region of interest, since then (25) and not (29) or (30) must be used. The

detuning Δ then serves to relate the position of say the peak of the lineshape L_d with respect to the Raman lines.

It is interesting to observe the duality between the two CARS techniques as exemplified by (27), (28) and (29), (30). Thus L_d and L_2 respectively play corresponding roles, in particular of determining the resolution. (This arises from the basic symmetry between the frequency pairs $-\omega_s$; ω_1 and $-\omega_2$; ω_{as}.) One consequence is that in later sections we need only calculate explicitly for one method, the result for the second following immediately. Of more importance is that experimentally, for the broadband method, only one laser (ω_2) need be narrow, instead of the two lasers (ω_1 and ω_s) in the scanning technique.

So far, only the three-laser configuration (ω_1, ω_s, ω_2 separate sources) sometimes known as four-colour CARS has been described. The most common experimental arrangement has in the past however used two lasers, one for both ω_1 and ω_2 and the other for the Stokes wave ω_s. To obtain the formulae corresponding to (25), it is necessary (see (23)) to deal with the fourth-order correlation function $\langle E_1(\omega_1)^* E_1(\omega_2)^* E_1(\omega_1') E_1(\omega_2')\rangle$. This is done in Appendix B, where it is shown that (25) again results, with subscripts 2 replaced by 1 and an overall factor of $\frac{1}{2}$ introduced into the right-hand side; we shall assume that this factor is incorporated in the definition of $\hat{I}_{as}$. Although of little (if any) experimental importance in CARS, the numerical factor is of some theoretical interest (see Appendix B). (In passing we note that the gaussian (normal) process assumption made for the laser spectra is only necessary for this case and the one below where a fourth-order correlation function is to be evaluated in terms of known second-order ones.)

The relative merits of these two- and three-laser CARS configurations have been discussed elsewhere [1–5] and so only the points for the two-laser arrangement that arise from spectral considerations need be raised here. First, in the scanning case *both* lasers must still be sharp, since ω_1 and ω_s contribute to L_d; the accompanying narrowness of ω_2 ($\equiv\omega_1$) is irrelevant, as shown above. Secondly, the broadband method has the complementary feature that ω_2 *alone* must be narrow whereas, since ω_1 ($\equiv\omega_2$) is then narrow, the broadness of L_d arises solely from the Stokes source ω_s. Thus, provided the Stokes source is sufficiently broad, broadband CARS with one narrow-band laser appears to have an advantage over scanning CARS with two. (It seems possible that the limited explanation of broadband CARS noted in the previous section arose from an examination of the two-laser scheme, whence a narrow ω_1 ($\equiv\omega_2$), though not necessary, was nevertheless the case.)

The above discussion leads to the interesting conclusion that another two-laser configuration could be used for the broadband technique, viz. one broad source for both ω_1 and ω_s, and a second, narrow, source for ω_2. Thus the pump (ω_1) and Stokes (ω_s) frequencies arise from within the linewidth of one laser. A linewidth of a few hundred wave-numbers compounded by the convolution implicit in L_d (26) could easily cover a large number of Raman lines of moderate shifts. The formula analogous to (25) again requires a fourth-order correlation function to be calculated (appendix B), with the result that in (25) the subscript s is replaced by 1 and the numerical factor of $\frac{1}{2}$ introduced as above.

A third CARS technique has been used [16], to investigate the effect of pressure on Raman linewidth. A broadband Stokes laser and a narrow-band

laser for both ω_1 and ω_2 were used (that is the two-laser broadband approach), but rather than resolve the antiStokes signal the total antiStokes intensity was measured as a function of pressure. Thus no spectral information is sought directly. A general expression for the antiStokes intensity $I_{as}{}^T$ is readily obtained from (29)

$$I_{as}{}^T = \int S_{as}(\omega_{as})\, d\omega_{as} = \hat{I}_{as} L_d(\omega_d{}^0) \int |L_\Gamma(\Delta)|^2\, d\Delta, \tag{31}$$

where the dummy variable has been denoted Δ to emphasize that all the Raman lines (for a suitably generalized L_Γ) are integrated over. Equation (31) shows that $I_{as}{}^T$ is independent of the linewidth of ω_2, as might be expected in view of the hybrid nature of (31), a combination of scanning and broadband methods. Thus two lasers, with a linewidth constraint on one only, that its spectrum should be constant over the Raman lines of interest, is sufficient. Moreover, if the Raman shifts lie within the broad laser's linewidth, then that laser could act for ω_1 and ω_s, rather than, as in [16], for ω_s alone. This would increase the available linewidth in L_d and thus enable more lines to be covered. One might be tempted to ask if *one* broad laser could directly act as a source for ω_1, ω_s and ω_2. The answer, as intuitively expected, is no. This is because in the liberal use of infinite integrations over frequency we have implicitly assumed that (*a*) the integrands are significant over limited spectral regions and that (*b*) the antiStokes spectral region is well separated from the frequencies ω_1, ω_s, ω_2. The latter is not possible using a single laser source.

The spectrum of the material excitation $S_Q(\omega_d)$ is also of some interest. Using (2), (11), (21) and (26), and recalling the notation $\omega_d = \omega_1 - \omega_s$, one soon finds

$$\begin{aligned} S_Q(\omega_d) &\equiv N \int \langle Q(\omega_d - \omega_d{}^0)^*\, Q(\omega_d + \omega - \omega_d{}^0) \rangle\, d\omega \\ &= \frac{N}{\eta_1{}^0 \eta_s{}^0} \left| \frac{\alpha_R}{2\epsilon_0 c\hbar} \right|^2 I_1 I_s \frac{L_d(\omega_d)}{(\Omega - \omega_d)^2 + \Gamma^2}. \end{aligned} \tag{32 a}$$

This may be rewritten in a number of ways. For example, the Raman susceptibility χ_R is defined by

$$\chi_R = \chi^{(3)}(-\omega_s;\ \omega_1,\ -\omega_1,\ \omega_s) = N|\alpha_R|^2/6\hbar\epsilon_0(\Omega + \omega_s - \omega_1 + i\Gamma),$$

whence

$$S_Q(\omega_d) = (-3\ \mathrm{Im}\ \chi_R I_1 I_s/2\eta_1{}^0\, \eta_s{}^0\, \epsilon_0 c\hbar\Gamma) L_d(\omega_d). \tag{32 b}$$

Alternatively, the peak stimulated Raman scattering gain coefficient g_R is given by

$$g_R = -3\omega_s{}^0\ \mathrm{Im}\ \hat{\chi}_R/\epsilon_0 c\hbar\eta_1{}^0\, \eta_s{}^0,$$

where $\hat{\chi}_R$ is the on-resonance Raman susceptibility, $\hat{\chi}_R = -iN|\alpha_R|^2/6\hbar\epsilon_0\Gamma$. In terms of g_R and using the definition (7 *c*)

$$S_Q(\omega_d) = \frac{g_R I_1 I_s}{2\hbar\omega_s{}^0\, \Gamma} L_d(\omega_d) |L_\Gamma(\Omega - \omega_d)|^2. \tag{32 c}$$

In this paper stimulated Raman processes are ignored and so $g_R I_1 z$ is assumed to be small, where z is the interaction length with the medium. Akhmanov and coworkers have studied the spectrum $S_Q(\omega_d, z)$ for stimulated Raman scattering, when $g_R I_1 z \sim 30$; see for example [8, 9].

Equation (32) shows that under conditions applying to CARS experiments the spectrum $S_Q(\omega_d)$ is simply the product of the driving-force spectrum $L_d(\omega_d)$ and the natural Raman lineshape $|L_\Gamma(\Omega-\omega_d)|^2$. Provided L_d is constant in the region of the Raman line (broadband excitation) the spectrum $S_Q(\omega_d)$ is just that of the Raman line. When $S_Q(\omega_d)$ is probed by a narrow ω_2, the antiStokes spectrum thus reproduces the Raman spectrum, as found earlier. For opto-acoustic spectroscopy the total acoustic energy, assumed proportional to $S_Q(\omega_d)$, is measured. Thus to resolve the spectrum requires that L_d be narrow, thereby selectively exciting the Raman line at frequency $\omega_d \simeq \omega_d{}^0$. Scanning ω_d causes the measured energy to follow the Raman spectrum.

The general conclusions of this section are summarized in the table.

4. Spectrum of an isolated line

Although, as remarked in the previous section, (25) and (26) provide a basis for analysing CARS spectra, detailed insight into these expressions cannot be obtained unless some specific laser lineshapes are introduced. Indeed for suitable analytic laser lineshapes simplified formulae may result which are more suitable for routine spectral analysis. To this end we now assume that the laser lineshapes may be satisfactorily approximated by either lorentzian or gaussian profiles. Theoretically a lorentzian profile would be generated by a laser of stable amplitude but exhibiting random phase fluctuations, for example an ideal cw laser, where photon noise results in phase diffusion [17]). (Similarly the absorption profile of an elastically pressure-broadened line is lorentzian.) A gaussian profile, on the other hand, arises purely from amplitude fluctuations. Most lasers will have photon statistics corresponding to a mixture of phase and amplitude fluctuations, and the appropriate approximating analytic lineshape to use should be determined by experiment.

The normalized lorentzian and gaussian lineshapes are, respectively,

$$\mathscr{L}_\Gamma(x)=(\Gamma/\pi)/(x^2+\Gamma^2)\,; \quad \int \mathscr{L}_\Gamma(x)\,dx=1 \tag{33}$$

and

$$\mathscr{G}_\Gamma(x)=(\tilde{\Gamma}\sqrt{\pi})^{-1}\exp(-x^2/\tilde{\Gamma}^2)\,; \quad \int \mathscr{G}_\Gamma(x)\,dx=1, \tag{34 a}$$

$$\tilde{\Gamma}\equiv\Gamma/\ln 2\simeq 1{\cdot}20\times\Gamma, \tag{34 b}$$

where Γ is the HWHM linewidth and $\tilde{\Gamma}$ denotes the $1/e$ halfwidth of the gaussian. Either or both of Γ and $\tilde{\Gamma}$ will be used whenever convenient and are always related by (34 *b*). To use (33) and (34) note that, for positive ω_1, $S_1(\omega_1)=\mathscr{L}_\Gamma(\omega_1-\omega_1{}^0)$ or $\mathscr{G}_\Gamma(\omega_1-\omega_1{}^0)$, where terms in $\mathscr{L}_\Gamma(\omega_1+\omega_1{}^0)$ and $\mathscr{G}_\Gamma(\omega_1+\omega_1{}^0)$ are negligible (cf. (2 *c*, *d*)); for negative ω_1 use $S_1(\omega_1)=S_1(-\omega_1)$.

We assume that the lasers have the same type of profile and so the driving-force spectrum L_d (26) is either

$$L_d(\omega_d)=\mathscr{L}_{\Gamma_d}(\omega_d-\omega_d{}^0)\,; \quad \Gamma_d=\Gamma_1+\Gamma_s, \quad \omega_d>0 \tag{35}$$

or

$$L_d(\omega_d)=\mathscr{G}_{\Gamma_d}(\omega_d-\omega_d{}^0)\,; \quad \Gamma_d=(\Gamma_1{}^2+\Gamma_s{}^2)^{1/2}, \quad \omega_d>0 \tag{36}$$

using the well known convolution properties of (33) and (34). The linewidth Γ_d is given by (35) or (36) depending on context. Thus a little care must be

Summary of CARS arrangements.

Method	Lasers	General requirement† (ω_1, ω_s)	General requirement† ω_d	General requirement† ω_2	Normal configuration† (ω_1, ω_s)	Normal configuration† ω_d	Normal configuration† ω_2	Comments
(*a*) Broadband	3	$\begin{pmatrix} *, & b \\ b, & * \end{pmatrix}$	*b*	*n*	$\begin{pmatrix} n, & b \\ b, & n \end{pmatrix}$	*b*	*n*	Only requirement is that ω_d be broad and ω_2 narrow.
(*b*) Broadband	2, $\omega_1 \equiv \omega_2$	(*n*, *b*)	*b*	*n*	(*n*, *b*)	*b*	*n*	ω_1 narrow by default, but unnecessary (see (*a*)).
(*c*) Broadband	2, $\omega_1 \equiv \omega_s$	(*b*, *b*)	*b*	*n*				Suitable for low-lying Raman lines, no laser tuning required.
(*d*) Integrated intensity	2, $\omega_1 \equiv \omega_2$, or 3	$\begin{pmatrix} *, & b \\ b, & * \end{pmatrix}$	*b*	*	(*n*, *b*)	*b*	*n*	The integrated intensity is measured and a broadband pump used ; therefore there is no resolution requirement and no need for narrow linewidth lasers.
	2, $\omega_1 \equiv \omega_s$	(*b*, *b*)	*b*	*				
(*e*) Scanning	3	(*n*, *n*)	*n*	*	(*n*, *n*)	*n*	*n*	Only require ω_d to be narrow.
(*f*) Scanning	2, $\omega_1 \equiv \omega_2$	(*n*, *n*)	*n*	*n*	(*n*, *n*)	*n*	*n*	ω_2 narrow by default, but unnecessary.
(*g*) Opto-acoustic	2 only, ω_1, ω_s	(*n*, *n*)	*n*					See § 3, phonon spectrum.

† *n*, narrow laser linewidth ; *b*, broad ; *, no requirement. Unless from one source, all waves should be spectrally separated. Source ω_d is the convolution of pump 1 and Stokes waves.

taken in comparing results, for given two lasers with linewidths Γ_1 and Γ_s the linewidth Γ_d differs depending on the chosen profile. The exceptions are for ω_1 sharp, that is $\Gamma_1 = 0$, when $\Gamma_d = \Gamma_s$ in either case, and conversely, if ω_s is sharp, then $\Gamma_d = \Gamma_1$.

Since the susceptibility profile is a lorentzian,

$$|\mathrm{L}_\Gamma(x)|^2 = \pi\Gamma\mathscr{L}_\Gamma(x) \tag{37}$$

then the intensity in the scanning method (27), for lorentzian laser profiles, is just

$$I_{as}^{\mathrm{L-L}}(\Delta) = \pi\Gamma\mathscr{L}_{\Gamma_{as}}(\Delta); \quad \Gamma_{as} = \Gamma_d + \Gamma, \tag{38}$$

again a lorentzian. (Here and subsequently we take $\hat{I}_{as} = 1$, since it is only a scaling factor.)

For a gaussian laser profile it is necessary to introduce the Voight profile. This well-known profile arises for example in the problem of Doppler-broadening of a lorentzian absorption lineshape and occurs here because (27) is formally the same problem. The profile will here be defined as

$$\mathscr{V}_{\Gamma(\Gamma_1,\Gamma_2)}(x) = \pi^{-3/2}\left(\frac{\Gamma_1}{\tilde{\Gamma}_2}\right)\int \frac{\exp(-t^2/\tilde{\Gamma}_2^2)}{(x-t)^2+\Gamma_1^2}\,dt, \tag{39 a}$$

$$\int \mathscr{V}_{\Gamma(\Gamma_1,\Gamma_2)}(x)\,dx = 1. \tag{39 b}$$

The linewidth Γ must be determined numerically as a function of Γ_1 and Γ_2; in the limit $\Gamma_2 \to 0$ it tends to Γ_1, and vice versa. The Voight profile is essentially the real part of the plasma dispersion function $w(z)$, which will be defined later

$$\mathscr{V}_{\Gamma(\Gamma_1,\Gamma_2)}(x) = (\tilde{\Gamma}_2\sqrt{\pi})^{-1}\,\mathrm{Re}\,w\left(\frac{x+i\Gamma_1}{\tilde{\Gamma}_2}\right). \tag{39 c}$$

The result analogous to (38) is thus

$$I_{as}^{\mathrm{L-G}}(\Delta) = \pi\Gamma\mathscr{V}_{\Gamma_{as}(\Gamma,\Gamma_d)}(\Delta). \tag{40}$$

A third combination of interest is where the lorentzian lineshape is replaced by a gaussian,

$$|\mathrm{L}_\Gamma(x)|^2 \to \pi\Gamma\mathscr{G}_\Gamma(x), \tag{41}$$

where $\int \pi\Gamma\mathscr{G}_\Gamma(x)\,dx = \pi\Gamma = \int |\mathrm{L}_\Gamma(x)|^2\,dx$. This substitution has no simple physical significance, but is an empirical analytical lineshape having the property that it falls off more rapidly than the lorentzian away from the line centre (that is as $|x|$ increases). In particular it does *not* represent a strongly Doppler-broadened line, since we are not replacing the dispersion function $(x-i\Gamma)^{-1}$ but rather its square modulus; the plasma dispersion function would be the appropriate substitution. Clearly, then, (41) cannot be used in a multiline spectrum where there is interference between the lines, as it does not derive from a dispersion function.

Using (41) and a gaussian laser profile in (27), one finds

$$I_{as}^{\mathrm{G-G}}(\Delta) = \pi\Gamma\mathscr{G}_{\Gamma_{as}}(\Delta); \quad \Gamma_{as} = (\Gamma_d^2 + \Gamma^2)^{1/2}. \tag{42}$$

Figure 2 depicts the antiStokes linewidth Γ_{as} as a function of the driving-force linewidth Γ_d for the above three models. It is seen that the rapid falling-off

in the wings of the gaussian laser profile results in an antiStokes linewidth which for moderate Γ_d is smaller than that for the purely lorentzian case. Moreover, the simple expression (42) gives a reasonable approximation to the mixed profile (39). Nevertheless a useful, and intuitively satisfying, rule of thumb is that the antiStokes linewidth is the sum of Γ and Γ_d.

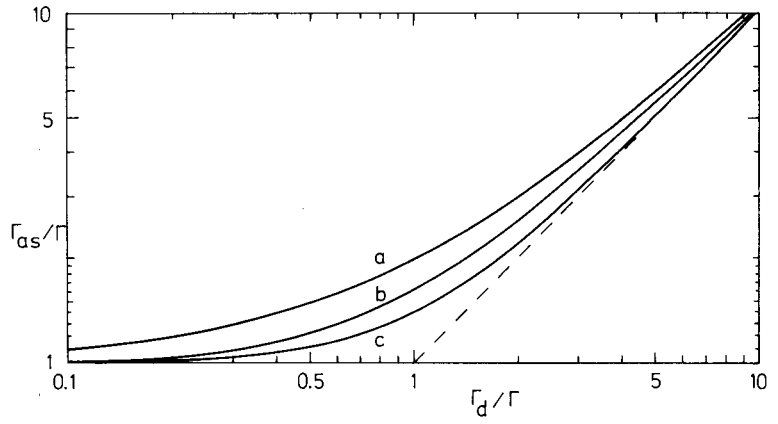

Figure 2. Observed antiStokes linewidth Γ_{as} of an isolated line as a function of the driving-force linewidth Γ_d in the scanning method. (In this and subsequent figures, replace Γ_d by Γ_2 for the corresponding broadband CARS result.) (*a*) lorentzian Raman and lorentzian laser lineshapes (L–L); (*b*) lorentzian Raman and gaussian laser lineshapes (L–G); (*c*) gaussian Raman and gaussian laser lineshapes (G–G).

These expressions are readily transcribed to produce the corresponding results for the idealized broadband method (29). For example, the result analogous to (38) is

$$S_{as}^{\mathrm{L-L}}(\omega_{as}) = \pi\Gamma\mathscr{L}_{\Gamma_d}(0)\mathscr{L}_{\Gamma_{as}}(\Delta+\omega_{as}^{0}-\omega_{as})$$
$$= (\Gamma/\Gamma_d)\mathscr{L}_{\Gamma_{as}}(\omega_{as}-\omega_{as}^{0}); \quad \Gamma_{as}=\Gamma_2+\Gamma, \tag{43}$$

where in the second step the unimportant overall shift Δ has been omitted and $\mathscr{L}_{\Gamma_d}(0)=1/\pi\Gamma_d$ inserted. Thus to find the antiStokes linewidth one need only replace Γ_d by Γ_2 in the expressions for Γ_{as} in (38), (40) and (42), and in figure 2. The antiStokes spectra are given in (43) and (45), (47) below.

When the driving-force spectrum is not constant over the spectral region of interest, (29) does not apply for the broadband method, and it is necessary to revert to the general formula (25). This may be evaluated for the three lineshape combinations treated above. However, for linewidths of hundreds of wavenumbers it is unlikely that a smooth single-peaked function will adequately describe the laser profile and the following formulae are at best indicative of the effect of a changing laser profile on the Raman spectrum. We quote only the L–G and G–G results, since the L–L expression is too cumbersome to be of any use here.

Thus

$$S_{as}^{\mathrm{L-G}}(\omega_{as}) = \frac{\Gamma\sqrt{\pi}}{\tilde{\Gamma}_{2d}} \exp\left(-\delta_{as}^{2}/\tilde{\Gamma}_{2d}^{2}\right)\mathscr{V}_{(\Gamma,\Gamma_2\Gamma_d/\Gamma_{2d})}(\eta_{2d}\delta_{as}-\Delta), \tag{44 a}$$

$$\Gamma_{2d}=(\Gamma_2^{2}+\Gamma_d^{2})^{1/2}; \quad \eta_{2d}=(1+\Gamma_2^{2}/\Gamma_d^{2})^{-1}=(\Gamma_d/\Gamma_{2d})^{2}, \tag{44 b}$$

where $\delta_{as}=\omega_{as}-\omega_{as}^{0}$. As $\Gamma_d\to\infty$

$$S_{as}^{\mathrm{L-G}}(\omega_{as})\sim(\Gamma\sqrt{\pi}/\tilde{\Gamma}_d)\mathscr{V}_{\Gamma_{as}(\Gamma,\Gamma_2)}(\delta_{as}-\Delta) \tag{45}$$

(cf. (43)), which is the result which would follow from a direct application of (29). Note that in (44 *a*) no linewidth for the Voight profile was defined, since we are interested in the antiStokes linewidth which results when δ_{as} is varied and this is influenced by the exponential factor.

Similarly

$$S_{as}^{\mathrm{G-G}}(\omega_{as})=\frac{\Gamma\ln 2}{(\Gamma^2\,\Gamma_d{}^2+\Gamma_2{}^2\,\Gamma_{0d}{}^2)^{1/2}}\exp\left[-\left\{\left(\frac{\delta_{as}-\eta_{0d}\Delta}{\tilde{\Gamma}_{as}}\right)^2+\left(\frac{\Delta}{\Gamma_{0d}}\right)^2\right\}\right], \tag{46 a}$$

$$\Gamma_{0d}=(\Gamma^2+\Gamma_d{}^2)^{1/2}\,;\quad \eta_{0d}=(1+\Gamma^2/\Gamma_{0d}{}^2)^{-1}=(\Gamma_d/\Gamma_{0d})^2, \tag{46 b}$$

$$\Gamma_{as}{}^2=\Gamma_2{}^2+\left(\frac{1}{\Gamma^2}+\frac{1}{\Gamma_d{}^2}\right)^{-1}=\Gamma_2{}^2+\eta_{0d}\Gamma^2. \tag{46 c}$$

When $\Gamma_d\to\infty$, then $\Gamma_{as}\to(\Gamma^2+\Gamma_2{}^2)^{1/2}$ and

$$S_{as}^{\mathrm{G-G}}(\omega_{as})\sim(\Gamma(\pi\ln 2)^{1/2}/\Gamma_d)\mathscr{G}_{\Gamma_{as}}(\delta_{as}-\Delta), \tag{47}$$

which again follows directly from (29). Equation (46) has the advantage of simplicity over (44) in that, for example, the antiStokes linewidth may be written down. The factor $\eta_{0d}\Delta$ follows directly from (32) as the shift in the peak of the excitation spectrum (a distortion) caused by a displaced driving-force spectrum. Hence for two isolated Raman lines, separated by α, the observed separation will be $\eta_{0d}\alpha$ and as $\Gamma<\Gamma_d$ in the broadband method then the relative error in observed separation will be $\eta_{0d}-1\simeq-(\Gamma/\Gamma_d)^2$. A >1 per cent error in observed line-spacing results if $\Gamma_d<10\Gamma$. From (46 *c*) one can estimate the error in observed antiStokes linewidth. Thus for $\Gamma_2\ll\Gamma$, as would be the case for high resolution, we have $\Gamma_{as}\simeq(\eta_{0d})^{1/2}\,\Gamma$ and so for $\Gamma<\Gamma_d$ the relative error in the observed width is $-\frac{1}{2}(\Gamma/\Gamma_d)^2$.

5. Multiline spectra

Although the spectrum of an isolated Raman line is of basic importance, the line spacing in the majority of molecular species is sufficiently small for there to be considerable interaction between them. This is of particular importance in CARS, where the dependence of the antiStokes signal on the square modulus of the non-linear susceptibility means that the interaction is of an interference nature. An associated interference effect, often important even for widely spaced lines, is due to the background contribution to the susceptibility from non-resonant Raman lines.

We modify the notation for the single-Raman line by extending (7). Thus for $\hat{\chi}_{\mathrm{CARS}}\mathrm{L}_\Gamma$ we write $\hat{\chi}_{\mathrm{CARS}}\to\bar{\chi}_{\mathrm{CARS}}$, where $\bar{\chi}_{\mathrm{CARS}}$ is an arbitrary constant with the dimensions of third order susceptibility and set L_Γ to

$$\mathrm{L}_\Gamma(\Omega+\omega_s-\omega_1)\to b+\sum_j a_j/(\Omega_j+\omega_s-\omega_1-i\Gamma_j). \tag{48}$$

The dimensionless parameters b and a_j/Γ_j represent the relative contributions from each line. Thus a_j is proportional to the population difference $N(\overline{\rho(g)}-\overline{\rho(f)})_j$ of the jth Raman line $g\to f$ and Ω_j and Γ_j are respectively its shift and

linewidth ; b is the background contribution. As in the previous section $\hat{I}_{as}$ is set equal to unity. Only the lorentzian dispersion function in (48) will be considered for the susceptibility ; it is suitable for a wide range of pressure-broadened lines and is in practice almost invariably used.

The scanning case (27) is straightforward if the laser profile is lorentzian. Thus after an elementary contour integration one has

$$I_{as}^{\mathrm{L-L}}(\Delta) = b^2 + 2\sum_j b a_j \,\mathrm{Re}\left(\frac{1}{\Delta_j - i\Gamma_{jd}}\right) + \sum_{jk} \frac{a_j a_k}{\Delta_{kj} + i(\Gamma_k + \Gamma_j)}\left[\frac{1}{\Delta - i\Gamma_{jd}} - \frac{1}{\Delta_k + i\Gamma_{kd}}\right], \quad (49)$$

where $\Gamma_{jd} = \Gamma_j + \Gamma_d$, $\Delta_{kj} = \Delta_k - \Delta_j$ and the detuning with respect to the jth line is

$$\Delta_j = \Delta + \Omega_j - \Omega_0 \; ; \quad \Delta = \Omega_0 + \omega_s{}^0 - \omega_1{}^0. \quad (50)$$

The detuning Δ is referenced to an arbitrary line 0. It is easily verified that for a single line and no background (49) reduces to (38) (set $b=0$, $a_j = \Gamma$). Similarly, if the linewidth Γ_d tends to zero, the right-hand side of (49) collapses to the square modulus of (48). Bearing in mind the non-dependence of $I_{as}(\Delta)$ on Γ_2, this result is then just the multiline extension of the monochromatic-wave result (17).

Equation (49) may be split into four parts. The first term is an additive and purely background contribution to the intensity. The second term arises from interference between each Raman line and the background. The third part is made up of isolated-line contributions ($j=k$ terms in the summation of the third term in (49)) and the fourth is made up of interference terms ($j \neq k$).

The magnitude of the pure background contribution is ultimately a limiting factor in the resolution of the resonant Raman lines. Given that there is a background, its importance is increased as Γ_d increases, since the other parts of (49) decrease as $1/\Gamma_d$. However, for high resolution Γ_d will be minimized by suitable choice of laser and thus the relative enhancement of the background is unlikely to be serious.

The effect of laser linewidth on the spectrum of a single line interacting with the background is particularly simple to analyse. Thus

$$I_{as}^{\mathrm{L-L}}(\Delta) \sim \frac{1}{\Gamma_{0d}}\left(\frac{1 + \lambda(\Delta/\Gamma_{0d})}{1 + (\Delta/\Gamma_{0d})^2}\right), \quad (51)$$

where $\lambda = b\Gamma/a_0$ is a dimensionless parameter which measures the importance of the background ; more precisely it is the ratio of background susceptibility to the peak value of the resonant part of the CARS susceptibility, $\chi_{\mathrm{NR}}/\hat{\chi}_{\mathrm{CARS}}$ in the notation of § 2. Apart from the appearance of $\Gamma_{0d} = \Gamma + \Gamma_d$ rather than Γ, this expression is identical to the usual monochromatic-wave formula [1–4] and exhibits the characteristic line asymmetry found in CARS. Since Δ is scaled by Γ_{0d} then the spectral characteristics such as the mean halfwidth $\bar{\Gamma}_{as}$ and the zero of (51) are precisely those of a Raman line of effective natural width Γ_{0d} and therefore the relative errors introduced by the finite laser linewidths are just Γ_d/Γ. For example, to order λ^2, $\bar{\Gamma}_{as} = \Gamma_{0d}(1 + \lambda^2/2)$ and the zero is at $\Delta = -\Gamma_{0d}/\lambda$.

The isolated-line contributions have been discussed in the previous section. The inter-line interference effects will be explored in the next sections; in general terms however (49) shows how the laser linewidth affects each line separately and that the interference is governed by the line spacing Δ_{kj}, independently of Γ_d.

For the broadband method (29) one need only replace Γ_{jd} in (49) by $\Gamma_{j2}=\Gamma_j+\Gamma_2$, multiply the whole by $L_d(0)=1/\pi\Gamma_d$ and suitably reword the foregoing account.

Possibly the most important analytic model is that based on gaussian laser spectra. To integrate (27) in this case requires the use of the plasma dispersion function [18] defined by

$$w(z)=\exp(-z^2)\left[1+\frac{2i}{\sqrt{\pi}}\int_0^z \exp(t^2)\,dt\right] \tag{52 a}$$

$$=\frac{i}{\pi}\int\frac{\exp(-t^2)}{z-t}\,dt\,;\quad \operatorname{Im} z>0, \tag{52 b}$$

$$w(z)=w(-z^*)^*\,;\quad \operatorname{Re} w(x+iy)=\operatorname{Re} w(-x+iy). \tag{52 c}$$

(Equation (52 b) may be used to verify (39).) Substitution of (48) into (27) and the use of the integral representation (52 b) leads to

$$I_{as}^{\mathrm{L-G}}(\Delta)=b^2-\frac{2\sqrt{\pi}}{\tilde{\Gamma}_d}\sum_j ba_j \operatorname{Im} w_j-\frac{\sqrt{\pi}}{\tilde{\Gamma}_d}\sum_{jk} a_j a_k \operatorname{Im}\left(\frac{w_j+w_k^*}{\Delta_{ki}+i(\Gamma_k+\Gamma_j)}\right), \tag{53 a}$$

$$w_j=w\left(\frac{-\Delta_j+i\Gamma_j}{\tilde{\Gamma}_d}\right). \tag{53 b}$$

The similarities between (53) and (49) are striking, essentially amounting to the replacement

$$(\Delta_j-i\Gamma_{jd})^{-1}\to(-\sqrt{\pi}/\tilde{\Gamma}_d)w_j.$$

For large z

$$w(z)\sim i\pi^{-1/2}/z. \tag{54}$$

Using (54) one can easily verify that (53) reduces correctly as $\Gamma_d\to 0$; for a single line with no background (53) reduces to (40) after using (39 c) and (52 c).

Again, the result for the idealized broadband case (29) follows directly from (53). The formula for the general broadband case (25), in which the driving-force spectrum need not be constant across the Raman spectrum can also be deduced and is

$$S_{as}^{\mathrm{L-G}}(\omega_{as})=[\exp(-\delta_{as}^2/\tilde{\Gamma}_{2d}^2)/\sqrt{(\pi)}\tilde{\Gamma}_{2d}]\left\{b^2-\frac{2\sqrt{(\pi)}\tilde{\Gamma}_{2d}}{\tilde{\Gamma}_2\tilde{\Gamma}_d}\sum_j ba_j \operatorname{Im}\bar{w}_j\right.$$

$$\left.-\frac{\sqrt{(\pi)}\tilde{\Gamma}_{2d}}{\tilde{\Gamma}_2\tilde{\Gamma}_d}\sum_{jk} a_j a_k \operatorname{Im}\left(\frac{\bar{w}_j+\bar{w}_k^*}{\Delta_{kj}+i(\Gamma_k+\Gamma_j)}\right)\right\}, \tag{55 a}$$

$$\bar{w}_j=w\left(\frac{\eta_{2d}\delta_{as}-\Delta_j+i\Gamma_j}{\tilde{\Gamma}_2\tilde{\Gamma}_d/\tilde{\Gamma}_{2d}}\right), \tag{55 b}$$

which may be compared with (44), in which the parameters η_{2d} and Γ_{2d} were defined; $\delta_{as}=\omega_{as}-\omega_{as}^0$.

The results of this section can be applied to the analysis of any multiline CARS spectrum provided the laser lineshapes are adequately modelled as gaussian or lorentzian. The plasma dispersion function is well tabulated (for example [18–20]) and efficient algorithms suited to computer computation exist (for example [18, 21, 22]).

In the next two sections some simple examples are presented, which have been chosen in order to assess the possible general effects of laser linewidth on complex CARS spectra, rather than with any particular molecule in mind.

6. Periodic spectrum

Surprisingly, there is at least one non-trivial example where a multiline spectrum can be analysed in detail without resort to extensive computation. This is for a periodic Raman spectrum, that is an infinite number of equally-spaced lines of equal strength and linewidth. (Tenuous contact with a real spectrum may be established by considering an O or S branch, at large J values and high temperature.)

This model has the further advantage that the molecule is completely characterized by only two parameters, the line spacing α and the linewidth Γ. For convenience we number the lines symmetrically about the centre line 0 and refer the detuning Δ to this line. Thus for monochromatic lasers the intensity for the scanning method is

$$I_{as}(\Delta) = \left| b + a \lim_{N\to\infty} \sum_{n=-N}^{N} (\Delta + n\alpha - i\Gamma)^{-1} \right|^2. \tag{56 a}$$

(Actually, as shown in § 3, (56) applies for any values of the linewidth Γ_2.) As shown in Appendix C, which also derives other formulae quoted in this section, (56 *a*) is just

$$I_{as}(\Delta) = \left| b + \frac{\pi a}{\alpha} \cot\left(\pi \frac{\Delta - i\Gamma}{\alpha}\right) \right|^2. \tag{56 b}$$

With no background ($b = 0$) this further simplifies to

$$I_{as}(\Delta) = \frac{\pi^2 a^2}{\alpha^2} \frac{\cosh(2\pi\Gamma/\alpha) + \cos(2\pi\Delta/\alpha)}{\cosh(2\pi\Gamma/\alpha) - \cos(2\pi\Delta/\alpha)}. \tag{57 a}$$

The peak antiStokes intensity is thus

$$I_{as}(0) = \frac{\pi^2 a^2}{\alpha^2} \coth^2\left(\frac{\pi\Gamma}{\alpha}\right) \tag{57 b}$$

and with (57 *a*) one finds the antiStokes linewidth

$$\Gamma_{as} = \frac{\alpha}{2\pi} \arccos\left\{\cosh(2\pi\Gamma/\alpha) \frac{3 - \cosh(2\pi\Gamma/\alpha)}{3\cosh(2\pi\Gamma/\alpha) - 1}\right\}. \tag{57 c}$$

The ratio of peak to minimum intensities is just $\coth^4(\pi\Gamma/\alpha)$ (the minimum intensity occurs at $\Delta = \alpha/2$) which is $< \frac{1}{2}$ for $\alpha/\Gamma \lesssim 2{\cdot}57$, and so for smaller line separations the lines merge and there is no halfwidth. Figure 3 depicts Γ_{as}/Γ as a function of α/Γ and one sees the breaking-off of the curve as α/Γ approaches $\sim 2{\cdot}57$. Interestingly, for most larger separations ($\alpha/\Gamma \gtrsim 2{\cdot}8$) the antiStokes

linewidth is actually slightly less than Γ. The reason for this is that the lines either side of 0 then contribute at a lower rate to the wings of 0 relative to its peak than the rate of fall-off of the contribution of 0 itself in its wings compared to its peak. This phenomenon is not solely an artefact of our model and occurs even in a three-line spectrum as also shown in figure 3. The effect is small, however, and expected to be unimportant experimentally except perhaps in those circumstances where precision measurements can be made.

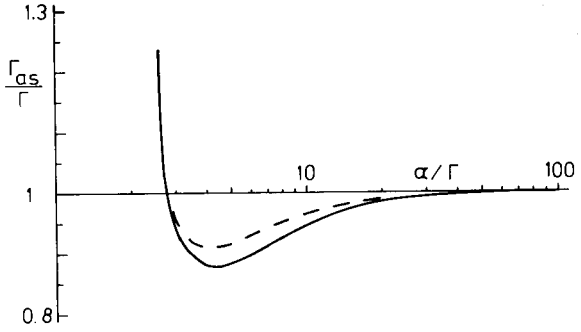

Figure 3. True antiStokes linewidth Γ_{as} of centre line of equally spaced lines of equal strength and linewidth versus the line separation α, for monochromatic lasers. Full curve, periodic spectrum (an infinite number of lines); broken curve, three lines.

If now the lasers have a finite linewidth Γ_d, then for a lorentzian one must use (49). Performing the summation gives

$$I_{as}^{\mathrm{L-L}}(\Delta) = b^2 + \frac{2\pi ba}{\alpha} \frac{\sin(2\pi\Delta/\alpha)}{\cosh(2\pi\Gamma_{0d}/\alpha) - \cos(2\pi\Delta/\alpha)} + \frac{\pi^2 a^2}{\alpha^2} \left(\frac{2\coth(2\pi\Gamma/\alpha)\sinh(2\pi\Gamma_{0d}/\alpha)}{\cosh(2\pi\Gamma_{0d}/\alpha) - \cos(2\pi\Delta/\alpha)} - 1 \right), \tag{58}$$

where $\Gamma_{0d} = \Gamma + \Gamma_d$ as usual. Using (58) it is possible to investigate the change in line asymmetry as a function of background strength and laser linewidth. Unlike a single Raman line interacting with a background (previous section) the line asymmetry does not scale independently with variations of $\lambda = b\Gamma/a$ and Γ_d. One can also rearrange (58) to find the antiStokes linewidth Γ_{as}, similarly to (57 *c*). In figure 4 we show Γ_{as} as a function of laser linewidth and line separation, but with no background. In addition, the corresponding curves for gaussian laser lineshapes are plotted, the result of a direct computation of (53). The curves terminate at the point where the lines merge, due to increasing laser linewidth. As is expected on the basis that the lorentzian lineshape has broader wings than the gaussian, for a given line separation the lines merge for smaller values of Γ_d in the former case. This is more pronounced for small separations (for example curves (*a*)), where the loss of resolution is more sensitive to variations in α and Γ_d. Similarly, the turnover from merged to isolated lines is more rapid in the gaussian case, where the true isolated-line curves are labelled (e), $\alpha/\Gamma = \infty$,

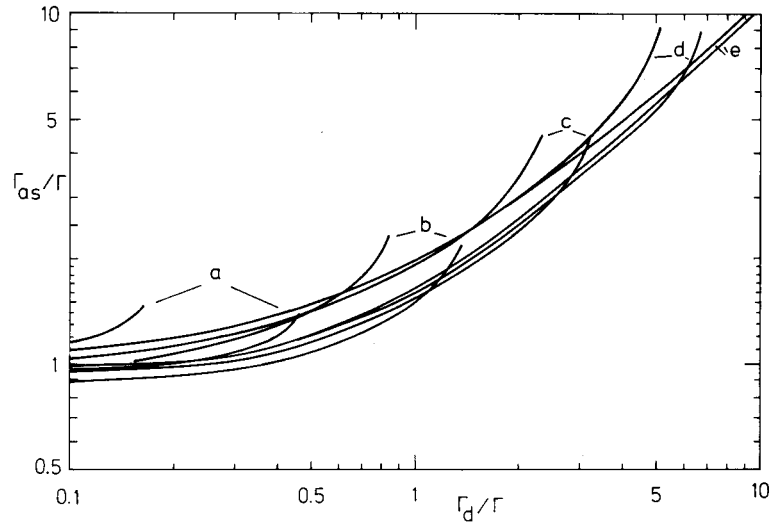

Figure 4. Observed antiStokes linewidth Γ_{as} in a periodic spectrum versus the driving-force linewidth Γ_d in the scanning method. Upper set of curves, lorentzian Raman and lorentzian laser lineshapes ; lower set of curves, lorentzian Raman and gaussian laser lineshapes. Line separations α/Γ are (*a*) 3, (*b*) 5, (*c*) 10, (*d*) 20, (*e*) ∞.

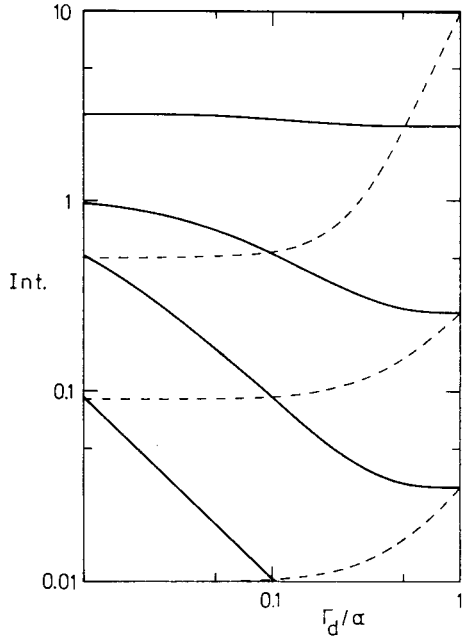

Figure 5. Peak intensity of line in a periodic spectrum relative to that of an isolated line of the same Raman linewidth Γ in the scanning method. Full curves, relative intensity with Γ/α as a parameter ; from top $\Gamma/\alpha=1$ (merged with upper x-axis), 0·5, 0·1, 0·01, 0·001. Broken curves, relative intensity with Γ_d/Γ as a parameter ; from top $\Gamma_d/\Gamma=1$, 10, 100.

and are the same as the ones depicted in figure 2 (*a*) for L–L and figure 2 (*b*) for L–G.

Finally, consider the peak intensity $I_{as}^{\mathrm{L-L}}(0)$ of a line in this periodic spectrum, relative to that of an isolated line excited by monochromatic lasers

$$g = I_{as}^{\mathrm{L-L}}(0)/(a^2/\Gamma^2)$$
$$= \frac{\pi^2\,\Gamma^2}{\alpha^2}\left[2\coth\left(\frac{2\pi\Gamma}{\alpha}\right)\coth\left(\frac{\pi\Gamma_{0d}}{\alpha}\right)-1\right]. \tag{59}$$

Figure 5 shows g as a function of Γ_d/α, with both Γ_d/Γ and Γ/α as parameters. When the line separation is large compared to both Γ and Γ_d, then $g \sim \Gamma/\Gamma_{0d}$, which is just the single-line relation (38) as expected. For finite line separations however the artificial nature of the infinite-line spectrum results in the intensity not decreasing indefinitely as Γ_d increases. Thus from (49) for sufficiently large Γ_d the intensity will vary as $1/\Gamma_d$, whereas from (59)

$$g \sim (2\pi^2\,\Gamma^2/\alpha^2)\coth(2\pi\Gamma/\alpha).$$

Nevertheless, for small values of Γ_d/α or Γ_d/Γ figure 5 has the characteristics of a real spectrum. Thus the laser linewidth has no effect until it is comparable to the Raman linewidth and then only if it approaches the line spacing. It is quite possible for the laser linewidth to exceed the line spacing, but not greatly affect the intensity so long as Γ_d/Γ is small.

7. Rotational contour fit

The last example to be treated in this paper is an attempt to assess the effect of laser linewidth on temperature measurements. If the lines are well separated, the problem is in principle trivial. Thus as seen in § 4 the peak of each line is scaled in the same way by the laser linewidth Γ_d (or Γ_2) and therefore the contour of the line peaks is independent of Γ_d provided Γ_d is larger than the variation in Raman linewidths from line to line. If the molecular population is confined to the lower levels of the Raman transitions, then (see (62) below) a plot of log (peak intensity of line) versus (energy of line) has slope $-1/kT$. This fact has been used in [6], for example, to deduce the temperature of H_2 gas. For most molecular species, however, there will be considerable interaction between the lines and it is necessary to analyse the spectrum in detail. The best fitting procedure to adopt is not clear at present, nor is it clear what influence the laser linewidth will have on the result. Thus, unlike the antiStokes linewidth that is observed for a particular line, the temperature that is deduced may depend on global features of the spectrum which are not sensitive to laser linewidths. The contour fit for isolated lines is indeed an example of this. We shall pursue the basic contour-fitting approach in this section, assuming for definiteness the scanning CARS technique ; one need only replace Γ_d by Γ_2 to obtain the corresponding result for the broadband CARS method.

Consider then the $v=0\rightarrow v=1$ branch of a diatomic molecule, for which the ground-state rotational energies are

$$E_0(J) = (B_e - \alpha_e/2)J(J+1) \simeq B_e J(J+1) \tag{60}$$

and the Q-branch shifts are

$$E_Q(J) = E_Q(0) - \alpha_e J(J+1). \tag{61}$$

The population probability $\overline{\rho(v=0, J)}$ of the lower state J is given by

$$\overline{\rho(v=0, J)} = (2J+1)g_I(J) \exp [-E_0(J)/kT], \tag{62}$$

where $g_I(J)$ is the nuclear spin degeneracy factor for level J. We assume that there is no background, no contribution from O and S branches, and no population in the upper Raman levels. Further, for typical non-resonant CARS experiments the normalized amplitudes a_j in (48) can be taken to be $a_j = \overline{\rho(v=0, J)}$ (we omit the slowly-varying J-dependent line strength factors) and as a first approximation the Raman linewidths are assumed equal. Despite these simplifications it is not possible to fully normalize the problem ; in particular there are two energy-level parameters, α_e ($\sim\alpha$ of the previous section) and B_e. We have therefore loosely based the calculations on N_2 gas by taking $B_e = 2$ cm^{-1}, $\alpha_e = 0{\cdot}02$ cm^{-1} and $g_I = 3$ (J odd) or 6 (J even). The assumption that there is no population in the upper Raman level means that the problem is limited to moderate temperatures (less than ~ 1000 K) but permits one to ignore the further complication of hot bands.

Figure 6 shows the result of trying to fit the usual monochromatic-wave formula, that is the susceptibility expression (48), to an observed spectrum by determining the least-squares fit at the rotational line peaks. The fit was obtained by varying the temperature T_{fit} and using the lines $Q(0)$ to $Q(30)$. (Thus to fit data g_i, $i=1, \ldots, N$, a function $\mu f_i(T)$ is tried. The scale factor μ

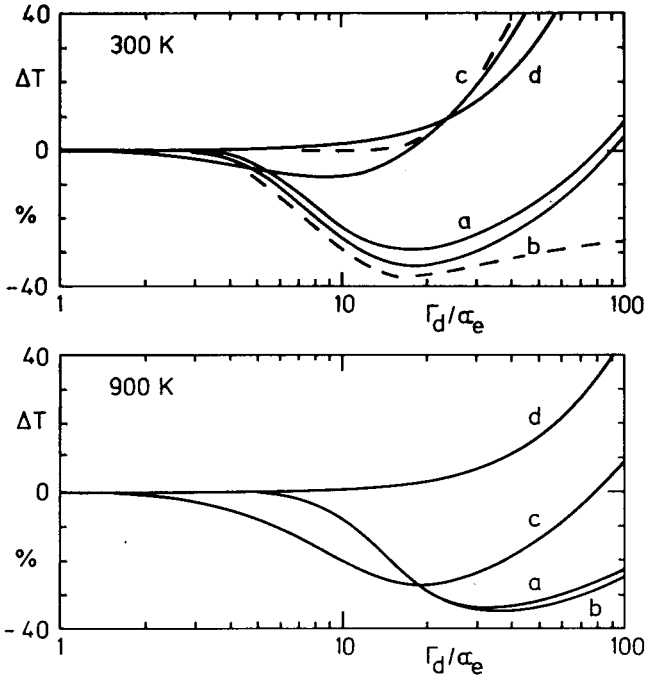

Figure 6. Error in temperature measurement resulting from fitting $Q(0)$–$Q(30)$ rotational contour without allowance for the driving-force linewidth Γ_d in the scanning method ; α_e is a rotational constant equal to half the spacing of the $Q(0)$–$Q(1)$ lines. Raman linewidths Γ/α_e are (*a*) 0·01, (*b*) 1·0, (*c*) 10, (*d*) 20, (*e*) 50. Broken curves, $\Gamma/\alpha_e = 1{\cdot}0$, negative error $Q(0)$–$Q(10)$ only, positive error $Q(20)$–$Q(30)$.

is given by $\mu(T)=(\Sigma_i g_i f_i)/(\Sigma_i f_i^2)$ and then T_{fit} is the solution of $\Sigma_i(\mu f_i - g_i)\,\partial f_i/\partial T=0$. These formulae follow by straightforward application of the least-squares principle.) The observed spectrum was calculated from (53) at a true temperature T and therefore allows for the effect of the laser linewidth (gaussian lineshape). Hence the relative error $\Delta T = T_{\text{fit}}/T - 1$ gives an estimate of the error in a temperature measurement that would be incurred if one tried to fit an observed spectrum without allowing for laser linewidth.

A qualitative impression of the observed spectrum may be obtained by noting that the line separation varies from $2\alpha_e = 0{\cdot}04$ cm^{-1} (lower lines $Q(0)$–$Q(10)$) to $\sim 60\alpha_e = 1{\cdot}2$ cm^{-1} (upper lines $Q(20)$–$Q(30)$) with a mean separation of $\sim 30\alpha_e = 0{\cdot}5$ cm^{-1} near the $Q(15)$ line. Thus for sharp Raman lines ($\Gamma/\alpha_e < 1$) the spectrum is well resolved when $\Gamma_d/\alpha_e < 1$, is unresolved for the lower lines when $\Gamma_d/\alpha_e \sim 10$ and is completely unresolved when $\Gamma_d \gtrsim 100$. This is the range of Γ_d values ($\sim 0{\cdot}02$ to 2 cm^{-1}) used in figure 6. The curves labelled (c) and (d) refer to the case where the Raman linewidth is large and therefore the lines are unresolved even for small laser linewidths.

The main features of these curves are easily explained. Consider first a molecule with sharp Raman lines (curve (a) $\Gamma = \alpha_e/100$). Thus for small laser linewidths the lines are essentially isolated and from (49) we can write

$$\Gamma_{0d}^2\, I_{as}^{\mathrm{L-L}}(\Delta=0) \simeq \ldots + a_{-1}^2/(1+\alpha^2/\Gamma_{0d}^2) + a_0^2 + a_1^2/(1+\alpha^2/\Gamma_{0d}^2) + \ldots \qquad (63)$$

for a typical peak intensity, where a_0^2 is the contribution from the line itself and $a_{\pm 1}^2/(1+\alpha^2/\Gamma_{0d}^2)$ give the contributions from adjacent lines separated by $\sim\alpha$. These adjacent lines are significant only when $\alpha/\Gamma_{0d} \lesssim 1$ and, as $\Gamma \ll \alpha$, we require $\Gamma_d \gtrsim \alpha$.

Now for the Q branch spectrum the lower lines are much more closely spaced than the higher ones and thus we can have $\Gamma_d \sim \alpha$ for the former but $\Gamma_d \ll \alpha$ for the latter. Hence the lower lines grow in intensity relative to the higher ones, which gives the impression of a lower temperature. This is the reason for the negative error shown for curves (a)–(c) in figure 6 and was confirmed by computing the fit with only the $Q(0)$–$Q(10)$ lines (dashed line in the figure).

As Γ_d increases, (63) tends to $\ldots + a_{-1}^2 + a_0^2 + a_1^2 + \ldots$ for the lower lines and the peak intensities for these stabilize with $\Gamma_d \gg \alpha_e$ but Γ_d comparable to the upper line spacings. Hence the upper lines now grow relative to the lower ones and the contour gives the impression of an increased temperature; as Γ_d increases the temperature error passes from negative to positive. The fit obtained with only the $Q(20)$ to $Q(30)$ lines confirms this (again shown as a dashed line in the figure). Finally, as Γ_d increases beyond the largest line spacings, the entire spectrum stabilizes in shape and the error becomes constant and positive. This was confirmed in the calculations, but not shown in the figure as this limit is of no practical interest (Γ_d several thousand α_e with no resolution of the spectrum).

If on the other hand the Raman linewidth is large (curve (d) $\Gamma = 50\alpha_e$) then from (63) we see that the contour over the lower lines will always be constant in shape, as $(\alpha/\Gamma_{0d})^2$ is less than $(\alpha/\Gamma)^2$ and $(\alpha/\Gamma)^2 \ll 1$. Thus the laser linewidth will only cause a relative increase in intensity for the higher lines and the error is therefore positive without a negative dip.

This discussion shows that the Q branch temperature analysis is sensitive to laser linewidth in a complicated mixture of positive and negative tendencies to

error. Since dye laser linewidths are typically 0·1 cm^{-1} and α_e is $\sim 0{\cdot}01$ cm^{-1}, then Γ_d/α_e is likely to be ~ 10 or greater. Then figure 6 shows that the error can be very large, even if $\Gamma_d \ll \Gamma$, unless there is a fortuitous cancellation in the distortion of the contour as the lower and upper lines change their relative intensities (for example curve (*c*)). The selection of, say, the upper or lower lines alone does not improve the situation. Thus except in the happy circumstances where the laser linewidths can be made narrower than Γ and possibly α_e, large and essentially indeterminate errors will occur if no account is taken of the effect of laser linewidth.

It is natural to consider if the position is made better by using the *S* (or O) branch. Here the lines are equally spaced by an amount $\sim 4B_e$, much larger than those in the *Q* branch. Hence there are no distortions incurred by non-uniform line spacings and *all* the lines remain effectively isolated if $\Gamma \ll B_e$, for much larger values of Γ_d than before.

It is however more difficult to determine the nature of the error qualitatively. Thus as Γ_d increases adjacent lines contribute as in (63), but simultaneously for all the lines in the spectrum. Because the intensity is stronger for the lower lines, then the absolute intensity changes will be largest for these. This might suggest an apparent drop in temperature. Direct computation shows however that the best fit occurs for increased temperature, since the broader maximum in the resultant contour allows more adjacent strong lines to contribute, thereby producing the required changes. It is seen therefore that the *S* (or O) branch contour, although weaker than the *Q* branch, is generally much less sensitive to laser linewidth because of both the uniformity and increased size of the line spacings.

8. Conclusions

In this paper we have considered the effect of finite laser linewidth on the CARS process in both general and specific terms, mainly under the assumption that the laser sources are monochromatic or may be approximated as stationary stochastic processes. The latter derives from the fact that most sources are far from transform limited and have linewidths due mainly to (quasi-) random amplitude and phase fluctuations.

The table summarizes the general conclusions (§ 3) in so far as they affect experiments in which high resolution of the Raman spectrum is required. The asterisks denote that there is no special laser linewidth requirement and comparison with the usual experimental configurations shows that in many cases the linewidth constraint on the sources is unnecessarily severe. For the two-laser arrangements (*b*) and (*f*) where one source plays the role of two, this is unavoidable and is possibly a secondary consideration compared to the simplicity of using only two lasers. However, three-laser configurations have the advantage, particularly for small Raman shifts, that the antiStokes frequency can be far removed from ω_1 and ω_s. It is therefore highly satisfactory to find that the additional laser need not have stringent linewidth requirements and on balance this may make the use of three lasers more attractive. Another possibility suited to small Raman shifts is the use of two lasers in the broadband technique, with one acting as both the first pump ω_1 and the *Stokes* wave ω_s ((*c*) in the table). Here there is no need for either laser to be tunable, the reproducibility from shot-to-shot is governed essentially by the single broadband

laser and ω_{as} can be far removed from ω_1 and $\omega_s \equiv \omega_1$. Thus advantages of conventional two- and three-laser configurations are combined.

The formulae derived in § 3 allow one to analyse a CARS spectrum given the laser and spontaneous Raman lineshapes. However, to gain insight and to reduce the computational burden, we introduced lorentzian and gaussian lineshape functions. Figure 2 shows the observed antiStokes linewidth for an isolated Raman line (§ 4). The multiline spectrum was also analysed, including an arbitrary background contribution, and compact working expressions derived (§ 5); the observed linewidth is not expected to be a simple function of laser linewidth and few general conclusions can be drawn.

As examples therefore these expressions were applied to a periodic spectrum (§ 6) and a Q-branch temperature problem (§ 7). The former has the advantage that the sum over all lines can be performed, resulting in a single-term formula for the intensity and observed linewidth. The laser linewidths affect the resolution only when they are comparable to or greater than the Raman linewidth, even if the latter exceeds the line spacing, as when the true spectrum is a band. The temperature analysis determined the error in measured temperature incurred by fitting a synthesized observed spectrum (measured with lasers of finite linewidth) with the ideal monochromatic-laser formula over the rotational contour. This showed the error to be a balance of negative and positive contributions due mainly to the relation of the laser linewidth to the non-uniform line spacings across the contour. For large spontaneous Raman linewidths Γ (rotational band) the net error was positive (increased temperature) and remained small until the laser linewidth approached Γ, even if greater than the line spacing (cf. above). The S or O branch measurements are less sensitive to a given laser linewidth, because of both the uniformity and increased magnitude of the line spacing, and the error when appreciable was positive. There is considerable scope for improving the fitting procedure, but it is clear that, excluding such ideal species as hydrogen, it will be necessary to take into account the laser linewidths if reliable results are to be obtained.

In summary then, we have derived a range of formulae which can be used to analyse CARS spectra when it is desired to take into account the effects of laser linewidth, which in turn are expected to be important for the majority of molecular species, both for Raman linewidth and temperature measurements. In the course of the calculations a number of important general conclusions were derived concerning the principal CARS configurations, with particular reference to constraints on laser linewidths.

The author is grateful to Professor I. R. Beattie, Dr. T. R. Gilson and particularly Dr. D. A. Greenhalgh for their interest in and constructive comments on this work. The author holds a Ramsay Memorial Fellowship and wishes to thank the Trustees for their support.

Appendix A

As pointed out in § 2, the material excitation approach to CARS, formulated in the time domain, is equivalent to the susceptibility approach, formulated in the frequency domain. The latter method is used in the body of this paper; here we indicate some corresponding equations in the time domain.

The starting equations are (9) and, corresponding to (13),

$$\frac{\partial}{\partial z}A_{as}(z,t)+\frac{\eta_{as}{}^0}{c}\frac{\partial}{\partial t}A_{as}(z,t)=\frac{i\omega_{as}{}^0}{2\epsilon_0 c}P_{as}(z,t)\exp(-ik_{as}{}^0 z)$$
$$=\frac{iN\omega_{as}{}^0\alpha_{\mathrm{CARS}}{}^*}{2\epsilon_0 c}Q(t)A_2(t)\exp(i\Delta k^0 z) \quad \text{(A 1)}$$

using (10). As in § 2, group velocity dispersion is ignored in (A 1). Changing to the characteristic coordinates $\zeta=z$ and $\tau=t-\eta_{as}{}^0 z/c$, (9) and (A 1) become

$$\frac{\partial}{\partial\tau}Q(\tau)+i(\Delta-i\Gamma)Q(\tau)=\frac{i\alpha_{\mathrm{R}}}{4\hbar}A_1(\tau)A_s(\tau)^*, \quad \text{(A 2)}$$

$$\frac{\partial}{\partial\zeta}A_{as}(\zeta,\tau)=\frac{iN\omega_{as}{}^0\alpha_{\mathrm{CARS}}{}^*}{2\epsilon_0 c}Q(\tau)A_2(\tau)\exp(i\Delta k^0\zeta). \quad \text{(A 3)}$$

Since $Q(-\infty)=A_{as}(0,\tau)=0$, the solution of (A 2)–(A 3) is

$$A_{as}(\zeta,\tau)=\frac{N\omega_{as}{}^0\alpha_{\mathrm{CARS}}{}^*}{2\epsilon_0 c\Delta k^0}[\exp(i\Delta k^0\zeta)-1]Q(\tau)A_2(\tau), \quad \text{(A 4)}$$

$$Q(\tau)=\frac{i\alpha_{\mathrm{R}}}{4\hbar}\int_{-\infty}^{\tau}\exp[i(\Delta-i\Gamma)(\tau'-\tau)]A_1(\tau')A_2(\tau')^*\,d\tau'. \quad \text{(A 5)}$$

These equations are analogous to (15).

Under the assumption that the fields $A_{1,2,s}$ are statistically independent and stationary, then

$$\langle A_{as}(\zeta,\bar\tau)^*A_{as}(\zeta,\bar\tau+\tau)\rangle=\left|\frac{N\omega_{as}{}^0\alpha_{\mathrm{CARS}}{}^*\alpha_{\mathrm{R}}}{2\epsilon_0 c\Delta k^0}\right|^2\sin^2(\Delta k^0\zeta/2)$$
$$\times\sigma_2(\tau)\int_{-\infty}^{\bar\tau}d\tau'\int_{\infty-}^{\bar\tau+\tau}d\tau''\exp[-i(\Delta+i\Gamma)(\tau'-\bar\tau)+i(\Delta-i\Gamma)(\tau''-\bar\tau-\tau)]$$
$$\times\sigma_1(\tau''-\tau')\sigma_s(\tau''-\tau')^*, \quad \text{(A 6)}$$

where for example

$$\sigma_1(\tau)=\langle A_1(\bar\tau)^*A_1(\bar\tau+\tau)\rangle \quad \text{(A 7)}$$

(cf. (20)). Making the substitutions $t'=\tau'-\bar\tau$ and $t''=\tau''-\bar\tau-\tau$ shows the antiStokes field to be stationary

$$\sigma_{as}(\tau)=\left|\frac{N\omega_{as}{}^0\alpha_{\mathrm{CARS}}{}^*\alpha_{\mathrm{R}}}{2\epsilon_0 c\Delta k^0}\right|^2\sin^2(\Delta k^0\zeta/2)$$
$$\times\sigma_2(\tau)\int_{-\infty}^{0}dt'\,dt''\exp[i(\Delta-i\Gamma)t''-i(\Delta+i\Gamma)t']$$
$$\times\sigma_1(t''-t'+\tau)\sigma_s(t''-t'+\tau)^*\,dt'\,dt''. \quad \text{(A 8)}$$

It is not difficult to show that, after taking Fourier transforms, (A 8) is equivalent to (24).

Appendix B

To evaluate the four-frequency correlation function

$$S_4(\omega_1,\omega_2,\omega_3,\omega_4)=\langle E(\omega_1)E(\omega_2)E(\omega_3)E(\omega_4)\rangle \quad \text{(B 1)}$$

we express it in terms of the four-time correlation

$$s_4(t_1, t_2, t_3, t_4) = \langle E(t_1)E(t_2)E(t_3)E(t_4)\rangle \tag{B 2}$$

using the transform relation (1)

$$S_4(\omega_1, \omega_2, \omega_3, \omega_4) = \left(\frac{1}{2\pi}\right)^4 \int \exp\left[i(\omega_1 t_1 + \ldots + \omega_4 t_4)\right] s_4(t_1, t_2, t_3, t_4)\, d^4 t, \tag{B 3}$$

where $d^4 t$ denotes $dt_1\, dt_2\, dt_3\, dt_4$. Under the assumption of a stationary and normal (gaussian) process, one has [14]

$$\begin{aligned} s_4(t_1, t_2, t_3, t_4) &= \tfrac{1}{8}\mathbf{S}_T{}^t\{\langle E(t_1)E(t_2)\rangle\langle E(t_3)E(t_4)\rangle\} \\ &= \tfrac{1}{8}\mathbf{S}_T{}^t\{s(t_2 - t_1)s(t_4 - t_3)\}, \end{aligned} \tag{B 4}$$

where $s(\tau) = s(-\tau) = \langle E(t)E(t+\tau)\rangle$ (cf. (20)) and $\mathbf{S}_T{}^t\{\ldots\}$ is an overall permutation operator instructing one to sum the expression in braces over all 4! permutations of $t_1 \ldots t_4$. We have required $E(t)$ to be a gaussian process in order that s_4 be expressible in terms of the known two-time correlations $s(\tau)$. (If s_4 is known but non-gaussian, then (B 3) gives the result directly.)

From (21) (but omitting the factor $\frac{1}{2}\epsilon_0 c\eta^0$ for clarity) $s(\tau)$ may be expressed in terms of the spectrum $S(\omega)$ (one is the Fourier transform of the other) and thus

$$\begin{aligned} S_4(\omega_1, \omega_2, \omega_3, \omega_4) = \tfrac{1}{8}\left(\frac{1}{2\pi}\right)^4 \int \exp\left[i(\omega_1 t_1 + \ldots + \omega_4 t_4)\right] S(\omega)S(\omega') \\ \times \mathbf{S}_T{}^t\{\exp\left[i\omega(t_1 - t_2) + i\omega'(t_3 - t_4)\right]\}\, d\omega\, d\omega'\, d^4 t. \end{aligned} \tag{B 4}$$

A little thought reveals that (B 4) is essentially unchanged if $\mathbf{S}_T{}^t$ is replaced by the permutation operator $\mathbf{S}_T{}^\omega$ which acts on $\omega_1, \ldots, \omega_4$

$$\begin{aligned} &S_4(\omega_1, -\omega_2, \omega_3, -\omega_4) \\ &\quad = \tfrac{1}{8}\left(\frac{1}{2\pi}\right)^4 \mathbf{S}_T{}^\omega \int S(\omega)S(\omega')\, \{\exp\left[i(\omega_1 + \omega)t_1 - i(\omega_2 + \omega)t_2\right. \\ &\qquad\qquad \left. + i(\omega_3 + \omega')t_3 - i(\omega_4 + \omega')t_4\right]\}\, d\omega\, d\omega'\, d^4 t \\ &\quad = \tfrac{1}{8}\mathbf{S}_T{}^\omega\{S(\omega_1)S(\omega_3)\delta(\omega_1 - \omega_2)\delta(\omega_3 - \omega_4)\}. \end{aligned} \tag{B 5}$$

Since $S(\omega) = S(-\omega)$, we can write

$$S_4(\omega_1, \omega_2, \omega_3, \omega_4) = \tfrac{1}{8}\mathbf{S}_T{}^\omega\{S(\omega_1)S(\omega_3)\delta(\omega_1 + \omega_2)\delta(\omega_3 + \omega_4)\} \tag{B 6}$$

$$\begin{aligned} &= S(\omega_1)[S(\omega_2)\delta(\omega_1 + \omega_4)\delta(\omega_2 + \omega_3) \\ &\quad + S(\omega_3)\delta(\omega_1 + \omega_2)\delta(\omega_3 + \omega_4) \\ &\quad + S(\omega_4)\delta(\omega_1 + \omega_3)\delta(\omega_2 + \omega_4)]. \end{aligned} \tag{B 7}$$

Thus the correlation function required in the text for conventional two-laser CARS is given by $S_4(-\omega_1, -\omega_2, \omega_1', \omega_2')$

$$\begin{aligned} &(\tfrac{1}{2}\epsilon_0 c\eta_1{}^0)^2\langle E_1(\omega_1)^* E_1(\omega_2)^* E_1(\omega_1')E_1(\omega_2')\rangle \\ &\quad = S_1(\omega_1)[S_1(\omega_2)\delta(\omega_1 - \omega_2')\delta(\omega_2 - \omega_1') + S_1(\omega_1')\delta(\omega_1 + \omega_2)\delta(\omega_1' + \omega_2') \\ &\qquad + S_1(\omega_2')\delta(\omega_1 - \omega_1')\delta(\omega_2 - \omega_2')]. \end{aligned} \tag{B 8}$$

When inserted into the equation analogous to (23), the middle part of (B 8) is found to make no contribution (the delta functions cannot be satisfied) and the remaining two parts make equal contributions. Bearing in mind the factor of $\frac{1}{4}$ due to the intensity of one beam playing two roles (§ 2), the result is just the right-hand side of (23) multiplied by $\frac{1}{2}$, and with $S_2(\omega_2)\to S_1(\omega_2)$. Similarly for the second two-laser scheme described in § 3, there is a numerical factor $\frac{1}{2}$ and $S_s(\omega_s)\to S_1(\omega_s)$.

If the mean intensity of the beam ω_1 were to be doubled so as to make the two-laser configuration more comparable to the three laser one, then it is seen that the former arrangement is intrinsically stronger by a factor of two. This is because for a single beam intensity fluctuations at ω_1 and ω_2 (or ω_s) occur simultaneously, whereas for three statistically independent lasers such coincidences are rare. The enhancement for these chaotic light beams is just that which gives rise to an $n!$ increase in the rate of n-photon absorption from a single chaotic light beam over that from n beams of the same mean intensity [17]; here $n=2$.

Appendix C

In this Appendix the infinite sums required for the periodic spectrum problem (§ 6) are evaluated. The basic sum is well-known (see for example [18, 23])

$$\lim_{N\to\infty}\sum_{n=-N}^{N}\frac{1}{n+z}=\frac{1}{z}+\sum_{n=1}^{\infty}\left(\frac{1}{n+z}+\frac{1}{-n+z}\right)=\pi\cot\pi z, \qquad \text{(C 1)}$$

from which (56 *b*) follows directly. Notice that it is not possible to write the first sum on the left-hand side of (C 1) simply as $\sum_{n=-\infty}^{\infty}$ since the sum is then undefined and need not converge. The limiting procedure ensures that to each positive term ($n>0$) there is a corresponding negative term ($-n$), as indicated in the second sum in (C 1), and the series is then well-defined and converges.

The need to impose a limiting procedure in (C 1) means that the calculation of (58) cannot be performed directly from (C 1) and (49). Thus (49) becomes

$$I_{as}(\Delta)=b^2+\frac{2\pi ba}{\alpha}\cot\pi\left(\frac{\Delta-i\Gamma}{\alpha}\right)+F, \qquad \text{(C 2)}$$

where F is formally defined as

$$F=\frac{1}{\alpha^2}\sum_{m,\,n=-\infty}^{\infty}\frac{1}{m-n+2i\Gamma/\alpha}\left(\frac{1}{n+(\Delta-i\Gamma_{0d})/\alpha}-\frac{1}{m+(\Delta+i\Gamma_{0d})/\alpha}\right). \qquad \text{(C 3)}$$

The first two parts of (C 2) give the corresponding parts of (58). F however cannot be summed by double application of (C 1) to the sums over m and n, since these are defined as tending to infinite limits *together* and therefore the finite double sum must first be found.

One way of summing F is to find an integral representation for the summands and reverse the order of integration and summation, providing suitable convergence tests are satisfied. This notion immediately indicates the method to

be used here, for we take the basic susceptibility (56 *a*), sum it as in (56 *b*) and insert this into the integral (27). The basic integral required is

$$I=\frac{c}{\pi}\int \frac{\cot \pi(z+a)\cot \pi(z+b)}{z^2+c^2}\,dz\,; \quad \mathrm{Re}\,c>0, \quad \mathrm{Im}\,-a,\,b>0. \qquad \text{(C 4)}$$

For $c=\Gamma_d/\alpha$, $a=b^*=(\Delta-i\Gamma)/\alpha$ one has $F=(\pi/\alpha)^2 I$. Equation (C 4) may be evaluated by contour integration, for which the contour is shown in figure 7. Thus in the upper half plane there is a simple pole at $z=ic$ and an infinite number of simple poles at $z=n-a$, $n=0, \pm 1, \ldots$. The contour chosen vanishes along A as $|z|\to\infty$ and along B and C as $N\to\infty$ (the contributions are $O(1/N^2)$). Hence, evaluating the residues

$$I=\cot \pi(a+ic)\cot \pi(b+ic)+\lim_{N\to\infty}\frac{2ic}{\pi}\sum_{n=-N}^{N}\frac{\cot \pi(b-a)}{(n-a)^2+c^2}.$$

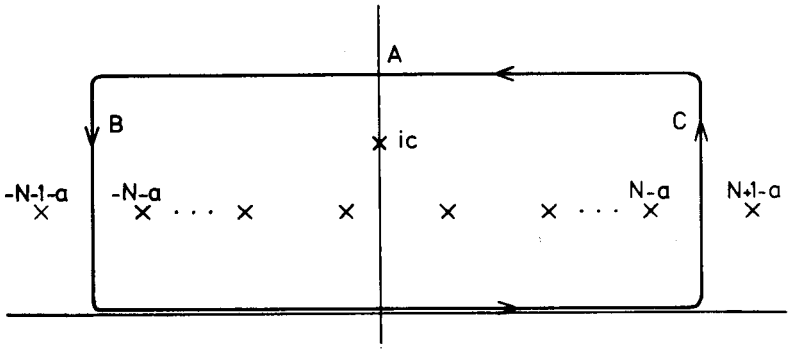

Figure 7. Contour for integration of equation (C 4).

The sum can be deduced from (C 1), whence, after some trigonometric manipulation,

$$I=\frac{\cot \pi(b-a)}{\cot \pi(b-a+2ic)}\left[\cot \pi(a-ic)\cot \pi(b+ic)+1\right]-1. \qquad \text{(C 5)}$$

This result leads directly to (58) after making the above indicated substitutions to find F.

References

[1] Akhmanov, S. A., and Koroteev, N. I., 1975, *Sov. Phys. JETP*, **40**, 650.
[2] Taran, J.-P., 1976, *Tunable Lasers and Applications*, edited by A. Mooradian, T. Jaeger and P. Stokseth (Springer-Verlag).
[3] Akhmanov, S. A., 1977, *Proc. Int. School of Physics 'Enrico-Fermi' Course* LXIV, *Nonlinear Spectroscopy*, edited by N. Bloembergen (North-Holland), p. 217.
[4] Nibler, J. W., Shaub, W. M., McDonald, J. R., and Harvey, A. B., 1978, *Vibrational Spectra and Structure : A Series of Advances*, Vol. 6, edited by J. R. Durig (Elsevier).
[5] Akhmanov, S. A., Koroteev, N. I., and Kholodnykh, A. I., 1974, *J. Raman Spectrosc.*, **2**, 239.
[6] Roh, W. B., Schreiber, P. W., and Taran, J.-P. E., 1976, *Appl. Phys. Lett.*, **29**, 174.
[7] Regnier, P. R., and Taran, J.-P. E., 1973, *Appl. Phys. Lett.*, **23**, 240.

[8] AKHMANOV, S. A., D'YAKOV, YU. E., and PAVLOV, L. I., 1974, *Sov. Phys. JETP*, **39,** 249.
[9] AKHMANOV, S. A., 1977, *Proc. Int. School of Physics 'Enrico-Fermi' Course*, LXIV, edited by N. Bloembergen (North-Holland), p. 255.
[10] HANNA, D. C., YURATICH, M. A., and COTTER, D., 1979, *Nonlinear Optics of Free Atoms and Molecules*, Springer Series in Optical Sciences (Springer-Verlag).
[11] YURATICH, M. A., and HANNA, D. C., 1977, *Molec. Phys.*, **33,** 671.
[12] SHEN, Y.-R., and BLOEMBERGEN, N., 1965, *Phys. Rev.* A, **137,** 1787.
[13] MAKER, P. D., and TERHUNE, R. W., 1965, *Phys. Rev.* A, **137,** 801.
[14] STRATONOVICH, R. L., 1963, *Topics in the Theory of Random Noise*, Vol. 1 (Gordon & Breach).
[15] KLAUDER, J. R., and SUDARSHAN, E. C. G., 1968, *Fundamentals of Quantum Optics* (Benjamin).
[16] SCHREIBER, P. W., and ROH, W. B., 1978, *Appl. Opt.*, **17,** 1418.
[17] LOUDON, R., 1973, *The Quantum Theory of Light* (Oxford University Press).
[18] ABRAMOWITZ, M., and STEGUN, I. A., 1970, *Handbook of Mathematical Functions* (Dover).
[19] FRIED, B. D., and CONTE, S. D., 1961, *The Plasma Dispersion Function* (Academic Press).
[20] FADDEEVA, V. N., and TERENT'EV, N. M., 1961, *Tables of Values of the Function* $w(z) = \ldots$ *for Complex Argument* (Pergamon).
[21] DRAYSON, S. R., 1976, *J. quant. Spectrosc. radiat. Transfer*, **16,** 611.
[22] GAUTSCHI, W., 1970, *SIAM Jl num. Analysis*, **7,** 187.
[23] BROMWICH, T. J. I'A., 1931, *An Introduction to the Theory of Infinite Series* (Macmillan).